Solvable 4D noncommutative QFT: phase transitions and quest for reflection positivity

Harald Grosse[1] and Raimar Wulkenhaar[2]

[1] *Fakultät für Physik, Universität Wien*
Boltzmanngasse 5, A-1090 Wien, Austria

[2] *Mathematisches Institut der Westfälischen Wilhelms-Universität*
Einsteinstraße 62, D-48149 Münster, Germany

Abstract

We provide further analytical and first numerical results on the solvable $\lambda\phi^4_4$-NCQFT model. We prove that for $\lambda < 0$ the singular integral equation has a unique solution, whereas for $\lambda > 0$ there is considerable freedom. Furthermore we provide integral formulae for partial derivatives of the matrix 2-point function, which are the key to investigate reflection positivity.

The numerical implementation of these equations gives evidence for phase transitions. The derivative of the finite wavefunction renormalisation with respect to λ is discontinuous at $\lambda_c \approx -0.39$. This leads to singularities in higher correlation functions for $\lambda < \lambda_c$. The phase $\lambda > 0$ is not yet under control because of the freedom in the singular integral equation.

Reflection positivity requires that the two-point function is Stieltjes. Implementing Widder's criteria for Stieltjes functions we exclude reflection positivity outside the phase $[\lambda_c, 0]$. For the phase $\lambda_c < \lambda \leq 0$ we show that refining the discrete approximation we satisfy Widder to higher and higher order. This is clear evidence, albeit no proof, of reflection positivity in that phase.

1 Introduction

The $\lambda\phi^4_4$-quantum field theory model [1] on noncommutative Moyal space has surprising properties. Although being the analogue of the ordinary $\lambda\phi^4_4$-model, it has vanishing β-function, which was (first perturbatively and after preliminary results in [2, 3]) proved by an ingenious combination of Ward identities related to a $U(\infty)$-symmetry with Schwinger-Dyson equations [4]. This method was extended in [5] to obtain a closed equation for the 2-point function of this model.

In our previous work [6] we have vastly extended the ideas of [5] in two directions. We showed that Ward identity and reality lead to an exact solution of the quartic matrix

[1] harald.grosse@univie.ac.at
[2] raimar@math.uni-muenster.de

model

$$\frac{1}{\text{volume}} \log \frac{\mathcal{Z}[E,J]}{\mathcal{Z}[E,0]}\,, \qquad \mathcal{Z}[E,J] = \int \mathcal{D}[\Phi]\ \exp(\mathrm{tr}(J\Phi - E\Phi^2 - \tfrac{\lambda}{4}\Phi^4)) \tag{1}$$

in terms of the solution of a non-linear equation. Here E represents an unbounded self-adjoint positive operator with compact resolvent, generalising the Laplacian, and J is a test function operator used to generate the correlation functions. Higher correlation functions are given by purely algebraic recursion formulae in terms of the eigenvalues of E and the solution of the non-linear equation for the 2-point function. We proved that any renormalisable quartic matrix model has vanishing β-function. The second extension achieved in [6] concerns the application to the noncommutative $\lambda\phi_4^4$-model [1] in the limit of extreme noncommutativity $\theta \to \infty$. We observed that the non-linear equation for the 2-point function can be split into a linear singular integral equation of Carleman type [7, 8] for the difference to the boundary and a resulting fixed-point problem

$$G_{b0} = G_{0b} = \frac{1}{1+b} \exp\left(-\lambda \int_0^b dt \int_0^{\Lambda^2} \frac{dp}{(\lambda\pi p)^2 + \left(t + \frac{1+\lambda\pi p \mathcal{H}_p^\Lambda[G_{\bullet 0}]}{G_{p0}}\right)^2} \right) \tag{2}$$

for the boundary 2-point function G_{a0}. Here $\mathcal{H}_p^\Lambda$ denotes the finite Hilbert transform over the interval $]0, \Lambda^2[$.

In recent work [10] we showed that the correlation functions of [6] lead to Schwinger functions for a scalar field on $\mathbb{R}^4$ which satisfy the easy Osterwalder-Schrader [11, 12] axioms (OS0) growth conditions, (OS3) permutation symmetry and, surprisingly for a highly noncommutative model, (OS1) Euclidean invariance. We further proved that (OS2) reflection positivity of the Schwinger 2-point function is equivalent to the requirement that the diagonal matrix 2-point function is a Stieltjes function [13].

A simple perturbative argument shows that reflection positivity does not hold for $\lambda > 0$ [10]. Looking closer at the possibility of $\lambda < 0$ we noticed that key formulae proved in [6] are only correct for $\lambda > 0$. In sec. 2.1 of this paper we carefully repeat this analysis for either sign of λ. As by-product we clarify the freedom resulting from the non-trivial solution of the homogeneous Carleman equation [8] which was left as an open problem in [6]. We prove the (lucky!) result that for $\lambda < 0$ (which could possibly be reflection positive) the Carleman equation has a unique solution, whereas for the less interesting case $\lambda > 0$ (no reflection positivity) there is considerable freedom.

The fixed point equation (2) resulted from a symmetry argument and not the true consistency equation for the boundary two-point function G_{a0}. It was so far unclear whether (2) admits false solutions which contradict the true consistency equation. In section 2.2 we close this gap and show that the true equation gives no further information.

In [14] we prove, using the Schauder fixed point theorem, that (2) has a solution (at least) for $-\frac{1}{6} \leq \lambda \leq 0$ inside the region $\exp(\mathcal{K}_\lambda)$, with

$$\mathcal{K}_\lambda = \left\{ f \in \mathcal{C}^1(\mathbb{R}_+) \ :\ f(0) = 0\,, \quad -\frac{1-|\lambda|}{1+x} \leq f'(x) \leq -\frac{1-\frac{|\lambda|}{1-2|\lambda|}}{1+x} \right\}. \tag{3}$$

The much simpler case $\lambda > 0$ was already treated in [6] under the (as we prove: false) assumption that the non-trivial solution of the homogeneous Carleman equation can be neglected.

A first hint about reflection positivity can be obtained from a computer simulation of the equations. Widder's criteria for Stieltjes functions [13] need derivatives of arbitrarily high order, which is impossible for a discrete approximation of the equation. We therefore derive in sec. 3 an integral formula for arbitrary partial derivatives of the 2-point function.

In sec. 4 we present first results of a numerical simulation of this model using *Mathematica*^{TM}. The source code is given in the appendix. Starting point is the fixed point equation (2) for the boundary 2-point function. We view G_{0b} as a piecewise-linear function and (2) as recursive definition of a sequence $\{G^i_{0b}\}_i$. We convince ourselves that this sequence converges in Lipschitz norm. For given λ, a sufficiently precise G^i_{0b} is then used to compute characterising data of the model. In this way we find clear evidence for a phase transition at $\lambda_c \approx -0.39$ where the function $\frac{\partial^2 G_{0b}(\lambda)}{\partial b \partial \lambda}\big|_{b=0}$ of λ is discontinuous. Within numerical error bounds we have[1] $G_{0b} \equiv 1$ for $0 \leq b < b_\lambda$ and $\lambda < \lambda_c$, which would imply that higher correlation functions do not exist for $\lambda < \lambda_c$. For $\lambda > 0$ we confirm an inconsistency due to neglecting the freedom with the homogeneous Carleman equation. This leaves the region $[\lambda_c, 0]$ as the only interesting phase, and precisely here we seem to have reflection positivity for the 2-point function. Of course, a discrete approximation by piecewise-linear functions cannot be Stieltjes. We show that the order where the Stieltjes property fails increases significantly when the approximation is refined; and this refinement slows down exactly at the same value $\lambda_c \approx -0.39$. We view this as overwhelming support for the conjecture that the boundary and diagonal 2-point functions G_{0b} and G_{aa}, respectively, are Stieltjes functions. Together with [10] this would imply reflection positivity of the Schwinger 2-point function.

2 The 2-point function revisited

In [6] we have studied the $\lambda\phi^4_4$-model on noncommutative Moyal space in matrix representation. We showed that the two-point function $G_{|\underline{ab}|}$ satisfies a closed non-linear equation in a scaling limit which simultaneously sends the volume $V = (\frac{\theta}{4})^2$ and the size $\mathcal{N}$ of the matrices to infinity with the ratio $\frac{\mathcal{N}}{\sqrt{V}} = \mu^2\Lambda^2(1+\mathcal{Y})$ fixed. In this limit, the 2-point function G_{ab} depends on 'continuous matrix indices' $a, b \in [0, \Lambda^2]$ and satisfies a non-linear integral equation $\mathcal{I}_a[G_{\bullet b}] = 0$. It was convenient to replace this equation by the coupled system $\mathcal{I}_a[G_{\bullet b}] - \mathcal{I}_a[G_{\bullet 0}] = 0$ and $\mathcal{I}_a[G_{\bullet 0}] = 0$. The difference equation admitted a wavefunction renormalisation $Z \mapsto (1+\mathcal{Y})$ which reduced the problem to a *linear singular integral equation* [7] for the difference $D_{ab} := a\frac{G_{ab}-G_{a0}}{b}$. We treat this equation an its solution $G_{ab}[G_{\bullet 0}]$ in sec. 2.1. In sec. 2.2 we show that the boundary equation $\mathcal{I}_a[G_{\bullet 0}] = 0$ gives no other information than the solution $G_{ab}[G_{\bullet 0}]$ plus symmetry $G_{ab} = G_{ba}$.

[1] We prove in the appendix of [14] that $G_{0b} = 1$ is an exact solution of (2) for any $\lambda < 0$ and $\Lambda^2 \to \infty$. This solution seems numerically unstable under small perturbations.

2.1 Solution of the Carleman equation for any sign of λ

As summarised above, the function $D_{ab} := a\frac{G_{ab}-G_{a0}}{b}$ derived from the 2-point function G_{ab} of self-dual noncommutative $\lambda\phi_4^4$-theory [1] in the limit of continuous matrix indices $a, b \in [0, \Lambda^2]$ satisfies [6] the Carleman singular integral equation [7]

$$\Big(\frac{b}{a} + \frac{1+\lambda\pi a\mathcal{H}_a^\Lambda[G_{\bullet 0}]}{aG_{a0}}\Big)D_{ab} - \lambda\pi\mathcal{H}_a^\Lambda[D_{\bullet b}] = -G_{a0}\ , \tag{4a}$$

$$\text{where} \qquad \mathcal{H}_a^\Lambda[f(\bullet)] = \frac{1}{\pi}\lim_{\epsilon\to 0}\Big(\int_0^{a-\epsilon} + \int_{a+\epsilon}^{\Lambda^2}\Big)dp\ \frac{f(p)}{p-a} \tag{4b}$$

denotes the *finite Hilbert transform* over the interval $]0, \Lambda^2[$.

The solution theory for such an equation over the interval $]-1, 1[$ was developed in Tricomi's book [8] and, in much larger generality, in [9]. Transforming the formulae given in [8] for $x \in]-1, 1[$ via $a = \frac{\Lambda^2}{2}(1+x)$ to $a \in]0, \Lambda^2[$ we have

Proposition 1 ([8, §4.4], $a = \frac{\Lambda^2}{2}(1+x)$**)** *Let $h \in \mathcal{C}(]0, \Lambda^2[)$ and $f \in L^q(]0, \Lambda^2[)$ for some $q > 1$ (depending on ϑ defined below). Then the singular integral equation*

$$h(a)\varphi(a) - \lambda\pi\mathcal{H}_a^\Lambda[\varphi(\bullet)] = f(a)\ , \qquad a \in]0, \Lambda^2[\ , \tag{5}$$

has the solution

$$\begin{aligned}\varphi(a) &= \frac{e^{-\mathcal{H}_a^\Lambda[\pi-\vartheta]}\sin(\vartheta(a))}{\lambda\pi a} \\ &\quad\times\Big(af(a)e^{\mathcal{H}_a^\Lambda[\pi-\vartheta]}\cos(\vartheta(a)) + \mathcal{H}_a^\Lambda\big[e^{\mathcal{H}_\bullet[\pi-\vartheta]}\bullet f(\bullet)\sin(\vartheta(\bullet))\big] + C'\Big) \qquad (6a)\\ &\overset{*}{=} \frac{e^{\mathcal{H}_a^\Lambda[\vartheta]}\sin(\vartheta(a))}{\lambda\pi}\Big(f(a)e^{-\mathcal{H}_a^\Lambda[\vartheta]}\cos(\vartheta(a)) + \mathcal{H}_a^\Lambda\big[e^{-\mathcal{H}_\bullet[\vartheta]}f(\bullet)\sin(\vartheta(\bullet))\big] + \frac{C}{\Lambda^2-a}\Big)\ , \qquad (6b)\end{aligned}$$

where C, C' are arbitrary constants and the angle ϑ is defined as $\vartheta(a) = \underset{[0,\,\pi]}{\arctan}\Big(\frac{\lambda\pi}{h(a)}\Big)$. This angle obeys the identities [8, §4.4(28)], [8, §4.4(18)] *and* [8, §4.4(20)],

$$e^{-\mathcal{H}_a^\Lambda[\vartheta]}\cos(\vartheta(a)) + \mathcal{H}_a^\Lambda\big[e^{-\mathcal{H}_\bullet^\Lambda[\vartheta]}\sin(\vartheta(\bullet)\big] = 1\ , \tag{7a}$$

$$e^{\mathcal{H}_a^\Lambda[\vartheta]}\cos(\vartheta(a)) - \mathcal{H}_a^\Lambda\big[e^{\mathcal{H}_\bullet^\Lambda[\vartheta]}\sin(\vartheta(\bullet))\big] = 1\ , \tag{7b}$$

$$\frac{e^{\mathcal{H}_a^\Lambda[\vartheta]}\cos(\vartheta(a))}{\Lambda^2-a} - \mathcal{H}_a^\Lambda\Big[\frac{e^{\mathcal{H}_\bullet^\Lambda[\vartheta]}\sin(\vartheta(\bullet))}{\Lambda^2-\bullet}\Big] = 0\ . \tag{7c}$$

The relation $\overset{*}{=}$ between (6a) and (6b) follows from $e^{-\mathcal{H}_a^\Lambda[\pi]} = \frac{a}{\Lambda^2-a}$ and consequently

$$\mathcal{H}_a^\Lambda[e^{\mathcal{H}_\bullet^\Lambda[\pi]}\bullet F(\bullet)] = \mathcal{H}_a^\Lambda[((\Lambda^2-a)-(\bullet-a))F(\bullet)] = ae^{\mathcal{H}_a^\Lambda[\pi]}\mathcal{H}_a^\Lambda[F(\bullet)] - \frac{1}{\pi}\int_0^{\Lambda^2}dp\ F(p)\ .$$

This means that if $p \mapsto F(p) = e^{-\mathcal{H}_p[\vartheta]} f(p)\sin(\vartheta(p))$ is integrable, (6a) and (6b) are equivalent with $C = C' - \frac{1}{\pi}\int_0^{\Lambda^2} dp\ F(p)$. The constants C, C' are possibly restricted by normalisation conditions which could prefer (6a) or (6b).

In [6] we have studied the solution of (4a) using (6b) under the assumption $C = 0$. In the meantime we noticed that for $\lambda < 0$ the normalisation conditions do not permit the step from (6a) to (6b). We carefully repeat the solution of (4a) based on (6a) and (6b) where C, C' are taken into account:

$$D_{ab} = -\frac{e^{-\mathcal{H}_a^\Lambda[\pi-\vartheta_b]}\sin(\vartheta_b(a))}{\lambda\pi a}\Big(aG_{a0}e^{\mathcal{H}_a^\Lambda[\pi-\vartheta_b]}\cos(\vartheta_b(a)) + \mathcal{H}_a^\Lambda\big[e^{\mathcal{H}_\bullet^\Lambda[\pi-\vartheta_b]}\bullet G_{\bullet 0}\sin(\vartheta_b(\bullet))\big] - C'_{b,\lambda,\Lambda^2}\Big) \tag{8a}$$

$$\stackrel{*}{=} -\frac{e^{\mathcal{H}_a^\Lambda[\vartheta_b]}\sin(\vartheta_b(a))}{\lambda\pi}\Big(G_{a0}e^{-\mathcal{H}_a^\Lambda[\vartheta_b]}\cos(\vartheta_b(a)) + \mathcal{H}_a^\Lambda\big[e^{-\mathcal{H}_\bullet^\Lambda[\vartheta_b]}G_{\bullet 0}\sin(\vartheta_b(\bullet))\big] - \frac{\Lambda^2 C_{b,\lambda,\Lambda^2}}{\Lambda^2 - a}\Big)\,, \tag{8b}$$

$$\vartheta_b(a) = \operatorname*{arctan}_{[0,\pi]}\Big(\frac{\lambda\pi a G_{a0}}{1 + bG_{a0} + \lambda\pi a\mathcal{H}_a^\Lambda\big[G_{\bullet 0}\big]}\Big)\,. \tag{8c}$$

Since b is merely a parameter for the function h in the Carleman equation, the constants C, C' are actually functions $C_{b,\lambda,\Lambda^2}, C'_{b,\lambda,\Lambda^2}$ of (b, λ, Λ^2). The starting point for the solution of (8a) or (8b) is the observation [6] that (8c) is, for $b = 0$, also a Carleman-type singular integral equation

$$\lambda\pi\cot\vartheta_0(a)G_{a0} - \lambda\pi\mathcal{H}_a^\Lambda[G_{a0}] = \frac{1}{a} \tag{9}$$

with solution

$$G_{a0} = \frac{e^{-\mathcal{H}_a^\Lambda[\pi-\vartheta_0]}\sin(\vartheta_0(a))}{\lambda\pi a}\big(e^{\mathcal{H}_a^\Lambda[\pi-\vartheta_0]}\cos(\vartheta_0(a)) + \mathcal{H}_a^\Lambda\big[e^{\mathcal{H}_\bullet^\Lambda[\pi-\vartheta_0]}\sin(\vartheta_0(\bullet))\big] + C'_{\lambda,\Lambda^2}\big) \tag{10a}$$

$$\stackrel{*}{=} \frac{e^{\mathcal{H}_a^\Lambda[\vartheta_0]}\sin(\vartheta_0(a))}{\lambda\pi}\Big(\frac{e^{-\mathcal{H}_a^\Lambda[\vartheta_0]}\cos(\vartheta_0(a))}{a} + \mathcal{H}_a^\Lambda\Big[\frac{e^{-\mathcal{H}_\bullet^\Lambda[\vartheta_0]}\sin(\vartheta_0(\bullet))}{\bullet}\Big] + \frac{\Lambda^2\tilde{C}_{\lambda,\Lambda^2}}{\Lambda^2 - a}\Big)\,. \tag{10b}$$

Writing $\sin(\vartheta_0(\bullet)) = \sin(\pi - \vartheta_0(\bullet))$ and $\cos(\vartheta_0(\bullet)) = -\cos(\pi - \vartheta_0(\bullet))$ in (10a) we can use (7b) to obtain $e^{\mathcal{H}_a^\Lambda[\pi-\vartheta_0]}\cos(\vartheta_0(a)) + \mathcal{H}_a^\Lambda\big[e^{\mathcal{H}_\bullet^\Lambda[\pi-\vartheta_0]}\sin(\vartheta_0(\bullet))\big] = -1$. The normalisation $G_{a0} = 1$ then forces $C'_{\lambda,\Lambda^2} - 1 = e^{\mathcal{H}_0^\Lambda[\pi-\vartheta_0]}\mathrm{sign}(\lambda)$ because $\lim_{a\to 0}\frac{\sin(\vartheta_0(a))}{|\lambda|\pi a} = 1$.

In (10b) we use rational fraction expansion $\mathcal{H}_a^\Lambda\Big[\frac{f(\bullet)}{\bullet}\Big] = \frac{1}{a}\Big(\mathcal{H}_a^\Lambda\big[f(\bullet)\big] - \mathcal{H}_0^\Lambda\big[f(\bullet)\big]\Big)$ as in [6] to obtain

$$G_{a0} = \frac{e^{\mathcal{H}_a^\Lambda[\vartheta_0]}\sin(\vartheta_0(a))}{\lambda\pi a}\Big(e^{-\mathcal{H}_a^\Lambda[\vartheta_0]}\cos(\vartheta_0(a)) + \mathcal{H}_a^\Lambda\Big[e^{-\mathcal{H}_\bullet^\Lambda[\vartheta_0]}\sin(\vartheta_0(\bullet))\Big] - \mathcal{H}_0^\Lambda\Big[e^{-\mathcal{H}_\bullet^\Lambda[\vartheta_0]}\sin(\vartheta_0(\bullet))\Big] + \frac{\Lambda^2 a\tilde{C}_{\lambda,\Lambda^2}}{\Lambda^2 - a}\Big)\,.$$

From (7a) we have $\mathcal{H}_a^\Lambda\big[e^{-\mathcal{H}_\bullet^\Lambda[\vartheta_0]}\sin(\vartheta_0(\bullet))\big]-\mathcal{H}_0^\Lambda\big[e^{-\mathcal{H}_\bullet^\Lambda[\vartheta_0]}\sin(\vartheta_0(\bullet))\big]=e^{-\mathcal{H}_0^\Lambda[\vartheta_0]}\cos(\vartheta_0(0))-e^{-\mathcal{H}_a^\Lambda[\vartheta_0]}\cos(\vartheta_0(a))$. From (8c) one concludes

$$\lim_{p\to 0}\vartheta_0(p)=\begin{cases}0 & \text{for } \lambda\geq 0\,,\\ \pi & \text{for } \lambda<0\,.\end{cases} \tag{11}$$

This means $\cos\vartheta_0(0)=\mathrm{sign}(\lambda)$ so that the two formulae (10a) and (10b) lead to

$$G_{a0}=\frac{e^{\mathcal{H}_0^\Lambda[\pi-\vartheta_0]-\mathcal{H}_a^\Lambda[\pi-\vartheta_0]}\sin(\vartheta_0(a))}{|\lambda|\pi a} \tag{12a}$$

$$\stackrel{*}{=}\frac{e^{\mathcal{H}_a^\Lambda[\vartheta_0]-\mathcal{H}_0^\Lambda[\vartheta_0]}\sin(\vartheta_0(a))}{|\lambda|\pi a}\Big(1+\frac{\Lambda^2 aC_{\lambda,\Lambda^2}}{\Lambda^2-a}\Big)\,. \tag{12b}$$

Both lines are *formally equivalent, but they rely on the existence of* $\mathcal{H}_0^\Lambda[\pi-\vartheta_0]$ *or* $\mathcal{H}_0^\Lambda[\vartheta_0]$. For given λ, this turns out to be the case only for one of the equations. The limit (11) implies $e^{-\mathcal{H}_0^\Lambda[\vartheta_0]}=\exp\big(-\frac{1}{\pi}\int_0^{\Lambda^2}\frac{dp}{p}\vartheta_0(p)\big)\stackrel{\lambda<0}{\longrightarrow}0$, which means that (12b) reduces for $\lambda<0$ to (12a) after undoing the (incorrect) step from $\tilde{C}_{\lambda,\Lambda^2}$ to C_{λ,Λ^2}. Similarly, $\lim_{a\to 0}e^{\mathcal{H}_a^\Lambda[\pi-\vartheta_0]}\stackrel{\lambda\geq 0}{=}\infty$, so that (12a) is only consistent with $\lambda<0$. These results can be summarised as follows:

Lemma 2

$$G_{a0}=\frac{e^{\mathcal{H}_0^\Lambda[\pi-\vartheta_0]-\mathcal{H}_a^\Lambda[\pi-\vartheta_0]}\sin(\pi-\vartheta_0(a))}{|\lambda|\pi a}\qquad \textit{for } \lambda<0\,, \tag{13a}$$

$$\stackrel{*}{=}\frac{e^{\mathcal{H}_a^\Lambda[\vartheta_0]-\mathcal{H}_0^\Lambda[\vartheta_0]}\sin(\vartheta_0(a))}{|\lambda|\pi a}\Big(1+\frac{\Lambda^2 aC_{\lambda,\Lambda^2}}{\Lambda^2-a}\Big)\qquad \textit{for } \lambda>0\,, \tag{13b}$$

where C_{λ,Λ^2} *is an arbitrary constant.* □

Let us introduce the new angle function

$$\tau_b(a):=\operatorname*{arctan}_{[0,\,\pi]}\left(\frac{|\lambda|\pi a}{b+\frac{1+\lambda\pi a\mathcal{H}_a^\Lambda[G_{\bullet 0}]}{G_{a0}}}\right)=\begin{cases}\vartheta_b(a) & \text{for } \lambda\geq 0\,,\\ \pi-\vartheta_b(a) & \text{for } \lambda<0\,.\end{cases} \tag{14}$$

We have $\tau_b(0)=0$ independent of the sign of λ, and Lemma 2 can be written in the unified from

$$G_{a0}=\frac{\sin(\tau_0(a))}{|\lambda|\pi a}\mathrm{e}^{\mathrm{sign}(\lambda)(\mathcal{H}_a^\Lambda[\tau_0]-\mathcal{H}_0^\Lambda[\tau_0])}\cdot\begin{cases}1 & \text{for } \lambda<0\,,\\ \big(1+\frac{\Lambda^2 aC_{\lambda,\Lambda^2}}{\Lambda^2-a}\big) & \text{for } \lambda>0\,.\end{cases} \tag{15}$$

In the next step we use the result of Lemma 2 to explicitly compute $G_{ab}=G_{a0}+\frac{b}{a}D_{ab}$ with D_{ab} given by (8a) and (8b), respectively. A key is the addition theorem

$$\lambda\pi a\sin\big(\vartheta_d(a)-\vartheta_b(a)\big)=(b-d)\sin\vartheta_b(a)\sin\vartheta_d(a) \tag{16}$$

obtained by insertion of (8c) into $\cot\vartheta_b(a)-\cot\vartheta_d(a)$. For $\lambda<0$ we thus have in (8a)

$$\begin{aligned}
G_{ab} &= G_{a0} - \frac{b\sin(\vartheta_b(a))e^{-\mathcal{H}^\Lambda_a[\pi-\vartheta_b]}}{\lambda\pi a^2}\Big(e^{\mathcal{H}^\Lambda_a[\pi-\vartheta_b]-\mathcal{H}^\Lambda_a[\pi-\vartheta_0]+\mathcal{H}^\Lambda_0[\pi-\vartheta_0]}\frac{\cos(\vartheta_b(a))\sin(\vartheta_0(a))}{|\lambda|\pi}\\
&\qquad + \frac{1}{|\lambda|\pi}\mathcal{H}^\Lambda_a\big[e^{\mathcal{H}^\Lambda_\bullet[\pi-\vartheta_b]-\mathcal{H}^\Lambda_\bullet[\pi-\vartheta_0]+\mathcal{H}^\Lambda_0[\pi-\vartheta_0]}\sin(\vartheta_0(\bullet))\sin(\vartheta_b(\bullet))\big] - C'_{b,\lambda,\Lambda^2}\Big)\\
&= \frac{e^{\mathcal{H}^\Lambda_0[\pi-\vartheta_0]-\mathcal{H}^\Lambda_a[\pi-\vartheta_0]}}{|\lambda|\pi a}\big(\sin\vartheta_0(a)-\cos\vartheta_b(a)\sin(\vartheta_0(a)-\vartheta_b(a))\big)\\
&- \frac{\sin(\vartheta_b(a))e^{\mathcal{H}^\Lambda_0[\pi-\vartheta_0]-\mathcal{H}^\Lambda_a[\pi-\vartheta_b]}}{|\lambda|\pi a^2}\mathcal{H}^\Lambda_a\big[e^{\mathcal{H}^\Lambda_\bullet[\vartheta_0-\vartheta_b]}(\bullet-a+a)\sin(\vartheta_0(\bullet)-\vartheta_b(\bullet))\big]\\
&+ C'_{b,\lambda,\Lambda^2}\frac{b\sin(\vartheta_b(a))e^{-\mathcal{H}^\Lambda_a[\pi-\vartheta_b]}}{\lambda\pi a^2}\\
&= \frac{\sin(\vartheta_b(a))e^{\mathcal{H}^\Lambda_0[\pi-\vartheta_0]-\mathcal{H}^\Lambda_a[\pi-\vartheta_b]}}{|\lambda|\pi a}\Big(1+\frac{\tilde{C}'_{b,\lambda,\Lambda^2}}{a}\Big)\,,
\end{aligned}\tag{17a}$$

where $\tilde{C}'_{b,\lambda,\Lambda^2}:=bC'_{b,\lambda,\Lambda^2}\,\mathrm{sign}(\lambda)e^{-\mathcal{H}^\Lambda_0[\pi-\vartheta_0]}-\frac{1}{\pi}\int_0^{\Lambda^2}dp\;e^{\mathcal{H}^\Lambda_p[\vartheta_0-\vartheta_b]}\sin(\vartheta_0(p)-\vartheta_b(p))$. We have used (7b) and standard trigonometric addition theorems to arrive at the last line of (17a). Existence of $\lim_{a\to0}G_{ab}$ imposes $\tilde{C}'_{b,\lambda,\Lambda^2}=0$.

For $\lambda>0$ we combine (8b) with (13b) to obtain

$$\begin{aligned}
G_{ab} &= G_{a0} - \frac{b\sin(\vartheta_b(a))e^{\mathcal{H}^\Lambda_a[\vartheta_b]}}{\lambda\pi a}\Big(\frac{e^{-\mathcal{H}^\Lambda_a[\vartheta_b]+\mathcal{H}^\Lambda_a[\vartheta_0]-\mathcal{H}^\Lambda_0[\vartheta_0]}}{|\lambda|\pi a}\Big(1+\frac{\Lambda^2aC_{\lambda,\Lambda^2}}{\Lambda^2-a}\Big)\sin\vartheta_0(a)\cos\vartheta_b(a)\\
&\quad + \frac{e^{-\mathcal{H}^\Lambda_0[\vartheta_0]}}{|\lambda|\pi}\mathcal{H}^\Lambda_a\Big[e^{\mathcal{H}^\Lambda_\bullet[\vartheta_0-\vartheta_b]}\frac{\sin(\vartheta_0(\bullet))\sin(\vartheta_b(\bullet))}{\bullet}\Big(1+\frac{\Lambda^2C_{\lambda,\Lambda^2}\bullet}{\Lambda^2-\bullet}\Big)\Big] - \frac{\Lambda^2C_{b,\lambda,\Lambda^2}}{\Lambda^2-a}\Big)\\
&= \frac{e^{\mathcal{H}^\Lambda_a[\vartheta_0]-\mathcal{H}^\Lambda_0[\vartheta_0]}}{|\lambda|\pi a}\Big(1+\frac{\Lambda^2aC_{\lambda,\Lambda^2}}{\Lambda^2-a}\Big)\Big(\sin\vartheta_0(a)-\cos\vartheta_b(a)\sin(\vartheta_0(a)-\vartheta_b(a))\Big)\\
&- \frac{e^{\mathcal{H}^\Lambda_a[\vartheta_b]-\mathcal{H}^\Lambda_0[\vartheta_0]}\sin(\vartheta_b(a))}{|\lambda|\pi a}\mathcal{H}^\Lambda_a\Big[e^{\mathcal{H}^\Lambda_\bullet[\vartheta_0-\vartheta_b]}\sin(\vartheta_0(\bullet)-\vartheta_b(\bullet))\Big(1+\frac{\Lambda^2C_{\lambda,\Lambda^2}(\bullet-\Lambda^2+\Lambda^2)}{\Lambda^2-\bullet}\Big)\Big]\\
&+ \frac{be^{\mathcal{H}^\Lambda_a[\vartheta_b]}\sin(\vartheta_b(a))}{\lambda\pi a}\frac{\Lambda^2C_{b,\lambda,\Lambda^2}}{\Lambda^2-a}\\
&= \frac{e^{\mathcal{H}^\Lambda_a[\vartheta_b]-\mathcal{H}^\Lambda_0[\vartheta_0]}\sin(\vartheta_b(a))}{|\lambda|\pi a}\Big(1-\Lambda^2C_{\lambda,\Lambda^2}-\frac{b\,\mathrm{sign}(\lambda)\Lambda^2C_{b,\lambda,\Lambda^2}e^{\mathcal{H}^\Lambda_0[\vartheta_0]}}{\Lambda^2-a}\Big)\,.
\end{aligned}\tag{17b}$$

To obtain the last line we have used both (7b) and (7c). The prefactor of $\big(1+\frac{\Lambda^2aC_{\lambda,\Lambda^2}}{\Lambda^2-a}\big)$ vanishes by trigonometric addition theorems. For $b=0$ the final formula must coincide with (13b) which imposes $C_{b,\lambda,\Lambda^2}=\mathrm{sign}(\lambda)e^{-\mathcal{H}^\Lambda_0[\vartheta_0]}\Big(\frac{\Lambda^2C_{\lambda,\Lambda^2}}{b}+f_{\lambda,\Lambda}(b)\Big)$, where $f_{\lambda,\Lambda}$ is an arbitrary function with $\lim_{b\to0}bf_{\lambda,\Lambda}(b)=0$.

We can summarise (17a) and (17b) and the corresponding discussion of the limit $a\to0$ in terms of the angle function $\tau_b(a)$ as follows:

Proposition 3 *In terms of the function $\tau_b(a)$ of the boundary 2-point function G_{a0}, see (14), the full 2-point function is given by*

$$G_{ab} = \frac{e^{\mathrm{sign}(\lambda)(\mathcal{H}^\Lambda_a[\tau_b]-\mathcal{H}^\Lambda_0[\tau_0])}\sin(\tau_b(a))}{|\lambda|\pi a}\cdot\begin{cases}\left(1+\frac{\Lambda^2(aC_{\lambda,\Lambda^2}+bf_{\lambda,\Lambda^2}(b))}{\Lambda^2-a}\right) & \text{for } \lambda>0\,,\\ 1 & \text{for } \lambda<0\,,\end{cases} \tag{18}$$

where C_{λ,Λ^2} is an arbitrary constant and f_{λ,Λ^2} an arbitrary function with $\lim_{b\to 0} bf_{\lambda,\Lambda}(b) = 0$. □

The limit $a \to 0$ of (18) reads

$$G_{0b} = \frac{e^{\mathrm{sign}(\lambda)(\mathcal{H}^\Lambda_0[\tau_b-\tau_0])}}{1+b}\cdot\begin{cases}\left(1+bf_{\lambda,\Lambda^2}(b)\right) & \text{for } \lambda>0\,,\\ 1 & \text{for } \lambda<0\,.\end{cases} \tag{19}$$

Proposition 3 fills a gap in [6]. We knew that the freedom parametrised by constants C, C' in the Carleman solution in Proposition 1 will influence the 2-point function, but we ignored this possibility in [6, Assumption 4.2]. Proposition 3 tells us that this Assumption is justified for $\lambda < 0$ provided that the angle function is suitably reflected $\vartheta_b(a) \mapsto \tau_b(a)$ for $\lambda < 0$ so that it vanishes at $a = 0$. This vanishing at 0 was used in the perturbative expansion [6, Appendix B] which agreed with a Feynman graph calculation. In terms of $\tau_b(a)$, agreement with the Feynman graph expansion shows that C_{λ,Λ^2} and f_{λ,Λ^2} are zero in perturbation theory. If these happen to be not identically zero (as we show by a numerical simulation), these must be flat functions of λ, i.e. all derivatives of $C_{\lambda,\Lambda^2}, f_{\lambda,\Lambda^2}$ with respect to λ vanish at $\lambda = 0$. This suggest a phase transition of infinite order $C_{\lambda,\Lambda^2}, f_{\lambda,\Lambda^2}\begin{cases}=0 & \text{for } \lambda\le 0\,,\\ \propto e^{-\frac{1}{\lambda}} & \text{for } \lambda>0\,.\end{cases}$

2.2 Consisteny relations for the boundary function G_{a0}

Equation (18) gives the full two-point function G_{ab} in terms of the boundary G_{a0}. The boundary function should be obtained from the equation symbolised by $\mathcal{I}_a[G_{\bullet 0}]$ in the introduction to sec. 2. This equation is [6, eqs. (4.33)+(4.17)]:

$$a - \frac{1}{G_{a0}} + 1 = -\frac{\lambda\int_0^{\Lambda^2} q\,dq\,(G_{aq}-G_{0q})}{1-\lambda\int_0^{\Lambda^2} dp\,G_{p0}} - \lambda\int_0^{\Lambda^2} dp\,\frac{a-a\frac{G_{p0}}{G_{a0}}}{(p-a)}\,, \tag{20}$$

which we rewrite as

$$\begin{aligned}&\Big((1+a)G_{a0}-1-\lambda\pi a\mathcal{H}^\Lambda_a[G_{\bullet 0}]\Big)\Big(1-\lambda\int_0^{\Lambda^2} dp\,G_{p0}\Big)\\ &= -\lambda G_{a0}\int_0^{\Lambda^2} q\,dq\,(G_{aq}-G_{0q}) - \lambda\pi a G_{a0}\mathcal{H}^\Lambda_a[1]\Big(1-\lambda\int_0^{\Lambda^2} dp\,G_{p0}\Big)\,.\end{aligned} \tag{21}$$

We show that this consistency condition gives no other information than symmetry $G_{ab} = G_{ba}$.

Lemma 4 *The solution (18) implies*

$$\lambda\pi\cot\vartheta_b(a)\cdot G_{ab}-\lambda\pi\mathcal{H}_a^\Lambda[G_{\bullet b}]=\frac{(1+b)G_{0b}}{a}\qquad or \tag{22a}$$

$$\lambda\pi a\big(G_{a0}\mathcal{H}_a^\Lambda[G_{\bullet b}]-G_{ab}\mathcal{H}_a^\Lambda[G_{\bullet 0}]\big)=b(G_{ab}-G_{0b})G_{a0}+(G_{ab}-G_{a0}G_{0b}) \tag{22b}$$

and

$$1+\lambda\int_0^\infty dp\;(G_{pb}-G_{p0})=(1+b)G_{0b}\;. \tag{23}$$

Proof. Let Θ be the step function $\Theta(\lambda)=1$ for $\lambda>0$ and $\Theta(\lambda)=0$ for $\lambda<0$. The Hilbert transform of (18) reads with (7) and rational fraction expansion

$$\begin{aligned}
\mathcal{H}_a^\Lambda[G_{\bullet b}] &= \Theta(\lambda)\frac{\cos\tau_b(a)\Lambda^2C_{\lambda,\Lambda^2}}{|\lambda|\pi(\Lambda^2-a)}\mathrm{e}^{\mathrm{sign}(\lambda)(\mathcal{H}_a^\Lambda[\tau_b]-\mathcal{H}_0^\Lambda[\tau_0])}\\
&+\frac{\mathrm{e}^{-\mathrm{sign}(\lambda)\mathcal{H}_0^\Lambda[\tau_0]}}{|\lambda|\pi a}\Big(\mathcal{H}_a^\Lambda\big[\sin(\tau_b(\bullet))\mathrm{e}^{\mathrm{sign}(\lambda)\mathcal{H}_\bullet^\Lambda[\tau_b]}(1+\Theta(\lambda)\tfrac{\Lambda^2bf_{\lambda,\Lambda^2}(b)}{\Lambda^2-\bullet})\big]\\
&\qquad-\mathcal{H}_0^\Lambda\big[\sin(\tau_b(\bullet))\mathrm{e}^{\mathrm{sign}(\lambda)\mathcal{H}_\bullet^\Lambda[\tau_b]}(1+\Theta(\lambda)\tfrac{\Lambda^2bf_{\lambda,\Lambda^2}(b)}{\Lambda^2-\bullet})\big]\\
&= \Theta(\lambda)\frac{\cos\tau_b(a)\Lambda^2C_{\lambda,\Lambda^2}}{|\lambda|\pi(\Lambda^2-a)}\mathrm{e}^{\mathrm{sign}(\lambda)(\mathcal{H}_a^\Lambda[\tau_b]-\mathcal{H}_0^\Lambda[\tau_0])}\\
&+\frac{\mathrm{e}^{-\mathrm{sign}(\lambda)\mathcal{H}_0^\Lambda[\tau_0]}}{|\lambda|\pi a}\Big(\mathrm{sign}(\lambda)\cos(\tau_b(a))\mathrm{e}^{\mathrm{sign}(\lambda)\mathcal{H}_a^\Lambda[\tau_b]}(1+\Theta(\lambda)\tfrac{\Lambda^2bf_{\lambda,\Lambda^2}(b)}{\Lambda^2-a})\\
&\qquad-\mathrm{sign}(\lambda)\mathrm{e}^{\mathrm{sign}(\lambda)\mathcal{H}_0^\Lambda[\tau_b]}(1+\Theta(\lambda)bf_{\lambda,\Lambda^2}(b))\\
&= \frac{\cos\vartheta_b(a)}{|\lambda|\pi a}\mathrm{e}^{\mathrm{sign}(\lambda)(\mathcal{H}_a^\Lambda[\tau_b]-\mathcal{H}_0^\Lambda[\tau_0])}\Big(1+\Theta(\lambda)\frac{\Lambda^2(C_{\lambda,\Lambda^2}a+bf_{\lambda,\Lambda^2}(b))}{\Lambda^2-a}\Big)\\
&-\frac{\mathrm{e}^{\mathrm{sign}(\lambda)(\mathcal{H}_0^\Lambda[\tau_b]-\mathcal{H}_0^\Lambda[\tau_0])}(1+\Theta(\lambda)bf_{\lambda,\Lambda^2}(b))}{\lambda\pi a}\\
&= \cot\vartheta_b(a)\cdot G_{ab}-\frac{(1+b)G_{0b}}{\lambda\pi a}\;,
\end{aligned} \tag{24}$$

which can be rearranged to (22a). We have used $\cos\tau_b(a)=\mathrm{sign}(\lambda)\cos\vartheta_b(a)$. Equation (22b) then results from (8c). Integration of (18) over $a=p$ gives with (7)

$$\begin{aligned}
&\int_0^{\Lambda^2}dp\;G_{pb}\\
&=\mathcal{H}_0^\Lambda\Big[\frac{\sin(\tau_b(\bullet))}{|\lambda|}\mathrm{e}^{\mathrm{sign}(\lambda)(\mathcal{H}_\bullet^\Lambda[\tau_b]-\mathcal{H}_0^\Lambda[\tau_0])}\Big(1+\Theta(\lambda)\Big(-C_{\lambda,\Lambda^2}\Lambda^2+\frac{\Lambda^2(C_{\lambda,\Lambda^2}\Lambda^2+bf_{\lambda,\Lambda^2}(b))}{\Lambda^2-\bullet}\Big)\Big)\Big]\\
&=\frac{\cos(\tau_b(0))}{\lambda}\mathrm{e}^{\mathrm{sign}(\lambda)(\mathcal{H}_0^\Lambda[\tau_b]-\mathcal{H}_0^\Lambda[\tau_0])}\big(1+\Theta(\lambda)bf_{\lambda,\Lambda^2}(b)\big)-\frac{(1-\Theta(\lambda)C_{\lambda,\Lambda^2}\Lambda^2)}{\lambda}\mathrm{e}^{-\mathrm{sign}(\lambda)\mathcal{H}_0^\Lambda[\tau_0]}\\
&=\frac{(1+b)G_{0b}}{\lambda}-\frac{(1-\Theta(\lambda)C_{\lambda,\Lambda^2}\Lambda^2)}{\lambda}\mathrm{e}^{-\mathrm{sign}(\lambda)\mathcal{H}_0^\Lambda[\tau_0]}\;.
\end{aligned} \tag{25}$$

Subtraction of the same equation at $b = 0$ gives the assertion (23). □

As by-product we obtain, setting $b = 0$ in (25), for the wavefunction renormalisation $Z(1+\mathcal{Y})$ given by [6, eq. (4.17)] the formula

$$\frac{1}{Z(1+\mathcal{Y})} = 1 - \lambda \int_0^{\Lambda^2} dp\, G_{p0} = \begin{cases} e^{\mathcal{H}_0^\Lambda[\tau_0]} & \text{for } \lambda < 0\,, \\ (1 - C_{\lambda,\Lambda^2}\Lambda^2) e^{-\mathcal{H}_0^\Lambda[\tau_0]} & \text{for } \lambda > 0\,. \end{cases} \tag{26}$$

This shows, in contrast to the interpretation in [6], that *Z is positive for $\lambda < 0$ (assuming $1+\mathcal{Y} > 0$) but negative for $\lambda > 0$ (assuming $C_{\lambda,\Lambda^2} = \mathcal{O}(1)$)*. We conclude that the 'wrong sign' $\lambda < 0$ is the good phase, and $\lambda > 0$ is the bad phase. This conclusion will repeatedly be confirmed throughout this paper.

We return to (21). Integrating (22b) over $b = q$ and multiplying by λ gives

$$\begin{aligned} &- \lambda G_{a0} \int_0^{\Lambda^2} dq\; q(G_{aq} - G_{0q}) + \lambda\pi a G_{a0} \mathcal{H}_a^\Lambda[\lambda \textstyle\int_0^{\Lambda^2} dq\; G_{\bullet q}] \\ &= (1 + \lambda\pi a \mathcal{H}_a^\Lambda[G_{\bullet 0}]) \lambda \int_0^{\Lambda^2} dq\; G_{aq} - \lambda G_{a0} \int_0^{\Lambda^2} dq\; G_{0q}\,. \end{aligned} \tag{27}$$

Let us define a function f by

$$\lambda \int_0^{\Lambda^2} dq\; G_{aq} =: f(a) + (1+a) G_{a0} - \Big(1 - \lambda \int_0^{\Lambda^2} dq\; G_{0q}\Big)\,. \tag{28}$$

For $f(a) = 0$ this is (23) for exchanged indices $G_{ab} \mapsto G_{ba}$. For the moment we keep $f(a)$ arbitrary in order to derive $f(a) = 0$ from (21). Equation (27) reads

$$\begin{aligned} &- \lambda G_{a0} \int_0^{\Lambda^2} dq\; q(G_{aq} - G_{0q}) - \Big(1 - \lambda \int_0^{\Lambda^2} dq\; G_{0q}\Big) \lambda\pi a G_{a0} \mathcal{H}_a^\Lambda[1] \\ &= -\lambda\pi a G_{a0} \mathcal{H}_a^\Lambda\big[f(\bullet) + (1+\bullet) G_{\bullet 0}\big] - \lambda G_{a0} \int_0^{\Lambda^2} dq\; G_{0q} \\ &+ (1 + \lambda\pi a \mathcal{H}_a^\Lambda[G_{\bullet 0}]) \Big(f(a) + (1+a) G_{0a} - \Big(1 - \lambda \int_0^{\Lambda^2} dq\; G_{0q}\Big)\Big)\,. \end{aligned} \tag{29}$$

This provides an alternative formula for the rhs of (21). Rewriting $\mathcal{H}_a^\Lambda[\bullet G_{\bullet 0}] = a\mathcal{H}_a^\Lambda[G_{\bullet 0}] + \frac{1}{\pi}\int_0^{\Lambda^2} dp\; G_{p0}$ and using the symmetry $G_{0p} = G_{p0}$ we arrive at

$$\begin{aligned} &\Big((1+a) G_{a0} - 1 - \lambda\pi a \mathcal{H}_a^\Lambda[G_{\bullet 0}]\Big)\Big(1 - \lambda \int_0^{\Lambda^2} dp\; G_{p0}\Big) \\ &= -\lambda\pi a G_{a0} \mathcal{H}_a^\Lambda[f(\bullet)] - \lambda\pi a(1+a) G_{a0} \mathcal{H}_a^\Lambda\big[G_{\bullet 0}\big] - \lambda(1+a) G_{a0} \int_0^{\Lambda^2} dp\; G_{p0} \\ &+ (1 + \lambda\pi a \mathcal{H}_a^\Lambda[G_{\bullet 0}]) \Big(f(a) + (1+a) G_{0a} - \Big(1 - \lambda \int_0^{\infty} dp\; G_{p0}\Big)\Big)\,, \end{aligned} \tag{30}$$

which reduces to

$$\lambda\pi \cot \vartheta_0(a) \cdot f(a) - \lambda\pi \mathcal{H}_a^\Lambda[f(\bullet)] = 0 \,. \tag{31}$$

In other words, the consistency equation (21) reduces to a homogeneous Carleman equation for $f(a)$. Symmetry $G_{ab} = G_{ba}$ implies $f(a) = 0$, and (31) is automatically fulfilled. Conversely, we proved in sec. 2.1 that for $\lambda < 0$ the homogeneous Carleman equation only has the trivial solution. For $\lambda > 0$ equation (31) could have solutions

$$f(a) = \tilde{C} \frac{\sin(\tau_b(a))}{|\lambda|\pi(\Lambda^2 - a)} \mathrm{e}^{\mathrm{sign}(\lambda)(\mathcal{H}_a^\Lambda[\tau_b] - \mathcal{H}_0^\Lambda[\tau_0])}$$

which contradict symmetry in case of $\tilde{C} \neq 0$. In summary, the consistency equation (21) contains no other information than (18) plus the symmetry requirement $G_{ab} = G_{ba}$.

Always for $\lambda < 0$ and for $\lambda > 0$ in a region (if existent) where $f_{\lambda,\Lambda^2} = 0$ we can use the symmetry requirement $G_{ab} = G_{ba}$, in particular $G_{0b} = G_{b0}$, to turn (19) into the fixed point problem

$$f_{\lambda,\Lambda^2} = 0 \quad \Rightarrow \quad G_{b0} = G_{0b} = \frac{1}{1+b} \exp\left(-\lambda \int_0^b dt \int_0^{\Lambda^2} \frac{dp}{(\lambda\pi p)^2 + \left(t + \frac{1+\lambda\pi p \mathcal{H}_p^\Lambda[G_{\bullet 0}]}{G_{p0}}\right)^2} \right) . \tag{32}$$

This formula holds independently of the sign of λ, and in this way we rigorously confirm [6, eq. (4.37)] for $\lambda < 0$. As shown in [14], (32) has for $-\frac{1}{6} \leq \lambda \leq 0$ a solution in $\exp \mathcal{K}_\lambda$, with $\mathcal{K}_\lambda$ given in (3). For $\lambda > 0$ but $f_{\lambda,\Lambda^2} = 0$, we can still use (32) to define G_{0b}, and the symmetry condition $G_{0a} = G_{a0}$ is actually an equation for the constant C_{λ,Λ^2}:

$$\begin{aligned} \frac{e^{-\mathcal{H}_0^\Lambda[\tau_0 - \tau_a]}}{1+a} &= \frac{e^{\mathcal{H}_a^\Lambda[\tau_0] - \mathcal{H}_0^\Lambda[\tau_0]} \sin(\tau_0(a))}{\lambda\pi a} \Big(1 + \frac{\Lambda^2 a C_{\lambda,\Lambda^2}}{\Lambda^2 - a} \Big) \\ \Rightarrow \qquad C_{\lambda,\Lambda^2} &= \Big(1 - \frac{a}{\Lambda^2} \Big) \frac{e^{\mathcal{H}_0^\Lambda[\tau_a] - \mathcal{H}_a^\Lambda[\tau_0]} \sqrt{\left(\frac{\lambda\pi a}{1+a}\right)^2 + \left(\frac{1+\lambda\pi a \mathcal{H}_a^\Lambda[G_{0\bullet}]}{(1+a)G_{0a}}\right)^2} - 1}{a} \,. \end{aligned} \tag{33}$$

If this is not a constant function of a, then the assumption $f_{\lambda,\Lambda^2} = 0$ was wrong.

3 Integral formulae for the derivative

3.1 Stieltjes functions

In [10] we have identified a limit in which the matrix correlation functions constructed in [6] converge to (connected) Schwinger functions in position space:

$$\begin{aligned} &\mathcal{S}_c(\mu x_1, \dots, \mu x_N) \\ &= \frac{1}{64\pi^2} \sum_{\substack{N_1 + \dots + N_B = N \\ N_\beta \text{ even}}} \sum_{\sigma \in \mathrm{S}_N} \Bigg(\prod_{\beta=1}^B \frac{4^{N_\beta}}{N_\beta} \int_{\mathbb{R}^4} \frac{dp_\beta}{4\pi^2\mu^4} \, e^{\mathrm{i}\left\langle \frac{p_\beta}{\mu}, \sum_{i=1}^{N_\beta} (-1)^{i-1} \mu x_{\sigma(N_1 + \dots + N_{\beta-1} + i)} \right\rangle} \Bigg) \\ &\quad \times G_{\underbrace{\frac{\|p_1\|^2}{2\mu^2(1+\mathcal{Y})}, \dots, \frac{\|p_1\|^2}{2\mu^2(1+\mathcal{Y})}}_{N_1} | \dots | \underbrace{\frac{\|p_B\|^2}{2\mu^2(1+\mathcal{Y})}, \dots, \frac{\|p_B\|^2}{2\mu^2(1+\mathcal{Y})}}_{N_B}} \,. \end{aligned} \tag{34}$$

Here, μ defines the mass scale so that (34) only involves densities, and $1+\mathcal{Y} := -\frac{dG_{0b}}{db}\big|_{b=0}$ is the finite wavefunction renormalisation. These Schwinger functions satisfy the Osterwalder-Schrader [12] axioms *(OS3) permutation symmetry* for trivial reasons but also *(OS1) Euclidean invariance*, which is highly surprising for a field theory on noncommutative Moyal space. The axiom *(OS4) clustering* is not satisfied, but also not strictly required.

In this section we prove integral equations for the partial derivatives $\frac{\partial^{n+\ell}G_{ab}}{\partial a^n \partial^\ell b}$ of the matrix 2-point function (18) assuming $C_{\lambda,\Lambda^2} = f_{\lambda,\Lambda^2} = 0$ (which is the case for $\lambda < 0$). On one hand this establishes explicit factorial growth $\left|\frac{\partial^{n+\ell}G_{ab}}{\partial a^n \partial^\ell b}\right| \leq C_{n\ell} n!\ell!$. Bounds on $C_{n\ell}$ are left for future work, but already at this point a bound of the type $\left|\frac{\partial^{n+\ell}G_{ab}}{\partial a^n \partial^\ell b}\right| \leq C(n!\ell!)^\alpha$ is plausible. Together with the recursion formulae for higher correlation functions [6], such bounds would be enough to prove the axiom *(OS0) growth conditions*.

In this paper we focus on another application of integral formulae for $\frac{\partial^{n+\ell}G_{ab}}{\partial a^n \partial^\ell b}$. We have shown in [10] that the Schwinger 2-point function satisfies the axiom *(OS2) reflection positivity* iff the diagonal matrix 2-point function $a \mapsto G_{aa}$ is a Stieltjes function, i.e.

$$G_{aa} = \int_0^\infty \frac{d\rho(t)}{a+t} \tag{35}$$

for some positive non-decreasing function ρ. This is essentially a consequence of the Källén-Lehmann spectral representation.

Stieltjes functions form an important subclass of the class $\mathcal{C}$ of *completely monotonic functions*. We refer to [15] for an overview about completely monotonic functions and their relations to other classes of functions. The class $\mathcal{C}$ characterises the positive definite functions on $\mathbb{R}_+$, i.e. for any $x_1, \ldots, x_n \geq 0$ the matrix $a_{ij} = f(x_i + x_j)$, with $f \in \mathcal{C}$, is positive (semi-)definite. A function $f : \mathbb{R}_+ \to \mathbb{R}$ is positive definite, bounded and continuous if and only if it is the Laplace transform of a positive finite measure, $f(x) = \int_0^\infty e^{-xt} d\mu(t)$. This representation provides a unique analytic continuation of such functions to the half space $\mathrm{Re}(z) > 0$. Remarkably, such analyticity is a consequence of the purely real conditions $(-1)^n f^{(n)}(x) \geq 0$ for all $n \in \mathbb{N}$ and $x > 0$.

The Stieltjes integral (35) provides a unique analytic continuation of a Stieltjes function to the cut plane $\mathbb{C} \setminus]-\infty, 0[$. Remarkably again, this analyticity can be tested by purely real conditions identified by Widder [13]: A smooth non-negative function f on $\mathbb{R}_+$ is Stieltjes iff $L_{n,t}[f(\bullet)] \geq 0$ for all $n \in \mathbb{N}$ and $t \in \mathbb{R}_+$, where $L_{0,t}[f(\bullet)] = f(t)$, $L_{1,t}[f(\bullet)] = \frac{d}{dt}\big(tf(t)\big)$ and

$$L_{n,t}[f(\bullet)] := \frac{(-t)^{n-1}}{n!(n-2)!} \frac{d^{2n-1}}{dt^{2n-1}} \big(t^n f(t)\big) \,, \qquad n \geq 2 \,. \tag{36}$$

If Widder's criterion is satisfied, the sequence $\{L_{n,t}[f(\bullet)]\}$ converges for $n \to \infty$ in distributional sense and almost everywhere to the measure function of the Stieltjes transform,

$$f(x) = \int_0^\infty \frac{\rho'(t)\, dt}{t+x} \,, \qquad \int_0^T \rho'(t)\, dt = \lim_{n\to\infty} \int_0^T dt\; L_{n,t}[f(\bullet)] \quad \text{a.e.} \,. \tag{37}$$

3.2 Derivatives of the 2-point function

In [16] we have given first results on $L_{n,t}[G_{\bullet\bullet}]$ based on numerically obtained interpolations and $n \leq 4$. For larger n this method becomes too noisy so that integral formulae for derivatives of G_{ab} become indispensable.

We start from (18) which we write for $C_{\lambda,\Lambda^2} = f_{\lambda,\Lambda^2}(b) = 0$, which is always the case for $\lambda < 0$, as

$$\begin{aligned}\log G_{ab} &= -\mathrm{sign}(\lambda)\mathcal{H}_0^\Lambda[\tau_0] + \mathrm{sign}(\lambda)\mathcal{H}_a^\Lambda[\tau_b] - \frac{1}{2}\log\Big((\lambda\pi a)^2 + \Big(b + \frac{1+\lambda\pi a\mathcal{H}_a^\Lambda[G_{\bullet 0}]}{G_{a0}}\Big)^2\Big) \\ &= -\mathrm{sign}(\lambda)\mathcal{H}_0^\Lambda[\tau_0] - \log(|\lambda|\pi a) + \mathrm{sign}(\lambda)\mathcal{H}_a^\Lambda[A(\cot\tau_b(\bullet))] + L(\cot\tau_b(a))\;, \qquad (38)\\ A(x) &:= \mathrm{arccot}(x) = \frac{\pi}{2} - \frac{1}{2\mathrm{i}}\Big(\log(1+\mathrm{i}x) - \log(1-\mathrm{i}x)\Big)\;, \\ L(x) &:= -\frac{1}{2}\log(1+x^2) = -\frac{1}{2}\Big(\log(1+\mathrm{i}x) + \log(1-\mathrm{i}x)\Big)\;.\end{aligned}$$

Here (14) has been used. For these functions A, L one has

Lemma 5 *The functions A, L introduced in (38) have the following ($k \geq 1$)-fold derivatives:*

$$A^{(k)}(\cot t) = (-1)^k(k-1)!\sin(kt)\sin^k t\;, \qquad L^{(k)}(\cot t) = (-1)^k(k-1)!\cos(kt)\sin^k t\;. \qquad (39)$$

Proof. An elementary calculation yields

$$\begin{aligned}\frac{d^k A(x)}{dx^k} &= \frac{(k-1)!(-1)^k}{(1+x^2)^k}\sum_{j=0}^{[\frac{k-1}{2}]}\binom{k}{2j+1}(-1)^j x^{k-2j-1}\;, \\ \frac{d^k L(x)}{dx^k} &= \frac{(k-1)!(-1)^k}{(1+x^2)^k}\sum_{j=0}^{[\frac{k}{2}]}\binom{k}{2j}(-1)^j x^{k-2j}\;.\end{aligned}$$

The assertion follows from the identities [17][§1.331.1+3],

$$\frac{\sin(kt)}{\sin^k t} = \sum_{j=1}^{[\frac{k-1}{2}]}\binom{k}{2j+1}(-1)^j\cot^{k-2j-1}t\;, \qquad \frac{\cos(kt)}{\sin^k t} = \sum_{j=0}^{[\frac{k}{2}]}\binom{k}{2j}(-1)^j\cot^{k-2j}t\;. \quad \square$$

The derivative $G_{ab}^{(n)} := \frac{d^n}{dt^n}G_{a+t,b+t}\big|_{t=0}$ will be traced back to

$$(\log G_{ab})^{(n)} := \frac{d^n}{dt^n}(\log G_{a+t,b+t})\Big|_{t=0} = \sum_{\ell=0}^{n}\binom{n}{\ell}\frac{\partial^n(\log G_{ab})}{\partial a^{n-\ell}\partial b^\ell}\;. \qquad (40)$$

This is achieved by Faà di Bruno's formula, i.e. the higher order analogue of the chain rule:

$$\frac{d^n}{dx^n}(g\circ f)(x)=\sum_{k=0}^{n} g^{(k)}(f(x))Y_{n,k}(f'(x),f''(x),\dots,f^{(n-k+1)}(x))\;, \tag{41}$$

where the $Y_{n,k}$ (also denoted $B_{n,k}$) are the Bell polynomials [18]

$$Y_{n,k}(x_1,\dots,x_{n-k+1})=\sum_{\substack{j_1+2j_2+\cdots=n\\ j_1+j_2+\cdots=k}}\frac{n!}{j_1!j_2!\cdots j_n!}\Big(\frac{x_1}{1!}\Big)^{j_1}\Big(\frac{x_2}{2!}\Big)^{j_2}\cdots\Big(\frac{x_{n-k+1}}{(n-k+1)!}\Big)^{j_{n-k+1}}\;. \tag{42}$$

For $n\geq 1$ the summation over k actually starts with $k=1$ because $Y_{n,0}=0$ for $n\geq 1$. In many cases it will be useful to include in (41) the case $n=0$ via the convention $Y_{0,0}=1$.

In a first step we have

$$G_{ab}^{(h)}=G_{ab}\sum_{k=0}^{h}Y_{h,k}\big(\{(\log G_{ab})^{(n)}\}_{n=1}^{h-k+1}\big)\;. \tag{43}$$

Since $\frac{\partial\cot\tau_b(a)}{\partial b}=\frac{1}{|\lambda|\pi a}$, Lemma 5 and (41) yield for (38)

$$\frac{\partial^\ell\log G_{ab}}{\partial b^\ell}\Big|_{\ell\geq 1}=\operatorname{sign}(\lambda)\,\mathcal{H}_a^\Lambda\Big[\frac{A^{(\ell)}(\cot\tau_b(\bullet))}{(|\lambda|\pi\bullet)^\ell}\Big]+\frac{L^{(\ell)}(\cot\tau_b(a))}{(|\lambda|\pi a)^\ell} \tag{44a}$$

$$=(-1)^\ell(\ell-1)!\operatorname{sign}(\lambda)\,\mathcal{H}_a^\Lambda\Big[\sin\big(\ell\tau_b(\bullet)\big)\Big(\frac{\sin\tau_b(\bullet)}{|\lambda|\pi\bullet}\Big)^\ell\Big]$$

$$+(-1)^\ell(\ell-1)!\cos\big(\ell\tau_b(a)\big)\Big(\frac{\sin\tau_b(a)}{|\lambda|\pi a}\Big)^\ell\;. \tag{44b}$$

For $a=0$ we obtain with $\lim_{a\to 0}\tau_b(a)=0$ and $\lim_{a\to 0}\frac{\sin\tau_b(a)}{|\lambda|\pi a}=\frac{1}{1+b}$ the equation

$$(\log G_{0b})^{(\ell)}:=\frac{d^\ell\log G_{0b}}{db^\ell}=\frac{(-1)^\ell(\ell-1)!}{(1+b)^\ell}+(-1)^\ell\ell!\lambda\int_0^{\Lambda^2}dp\,\frac{\sin\big(\ell\tau_b(p)\big)}{\ell|\lambda|\pi p}\Big(\frac{\sin\tau_b(p)}{|\lambda|\pi p}\Big)^\ell\;. \tag{45}$$

The asymptotic similarity of the functions G_{aa} and G_{0a} (see Section 4) lets us conjecture that $a\mapsto G_{aa}$ is Stieltjes iff $b\mapsto G_{0b}$ is Stieltjes. Stieltjes functions are logarithmically completely monotonic [15], i.e.

$$f(x)=\int_0^\infty\frac{d\rho(t)}{x+t}\qquad\Rightarrow\quad(-1)^n\frac{d^n}{dx^n}(\log f(x))\geq 0\;. \tag{46}$$

Therefore, necessary for $b\mapsto G_{0b}$ being a Stieltjes function is $(-1)^\ell(\log G_{0b})^{(\ell)}\big|_{b=0}\geq 0$ or $\mathcal{Y}_\ell\geq -1$ for all ℓ, where

$$\mathcal{Y}_\ell:=\lambda\int_0^{\Lambda^2}dp\,\frac{\sin\big(\ell\tau_0(p)\big)}{|\lambda|\pi p}\Big(\frac{\sin\tau_0(p)}{|\lambda|\pi p}\Big)^\ell=\operatorname{sign}(\lambda)\mathcal{H}_0^\Lambda\Big[\sin(\ell\tau_0(\bullet))\Big(\frac{\sin\tau_0(\bullet)}{|\lambda|\pi\bullet}\Big)^\ell\Big]\;. \tag{47}$$

In particular, $\mathcal{Y}_1 =: \mathcal{Y}$ is the finite wavefunction renormalisation [6, eq. (4.30)].

Differentiation of the Hilbert transform (4b) leads after integration by parts to

$$\begin{aligned}\frac{d}{da}\mathcal{H}^\Lambda_a[f(\bullet)] &= \frac{1}{\pi}\lim_{\epsilon\to 0}\Big(\frac{f(a-\epsilon)}{a-\epsilon-a} - \frac{f(a+\epsilon)}{a+\epsilon-a} + \Big(\int_0^{a-\epsilon} + \int_{a+\epsilon}^{\Lambda^2}\Big)\frac{f(p)dp}{(p-a)^2}\Big)\\ &= -\frac{f(0)}{\pi a} - \frac{f(\Lambda^2)}{\pi(\Lambda^2-a)} + \mathcal{H}^\Lambda_a[f'(\bullet)] \qquad (48a)\\ &= -\frac{f(\Lambda^2)}{\pi a} + \frac{1}{\pi a}\int_0^{\Lambda^2} dp\; f'(p)\frac{p-a}{p-a} - \frac{f(\Lambda^2)}{\pi(\Lambda^2-a)} + \frac{1}{a}\mathcal{H}^\Lambda_a[af'(\bullet)]\\ &= -\frac{f(\Lambda^2)}{\pi a(1-\frac{a}{\Lambda^2})} + \frac{1}{a}\mathcal{H}^\Lambda_a[\bullet f'(\bullet)]\;. \qquad (48b)\end{aligned}$$

The two equations (48a) and (48b) are equivalent, but in the numerical simulation one of them is preferred. We can only use (48a) for higher derivatives as long as $f^{(k)}(0)$ exists. Such existence could rely on cancellations which are numerically not guaranteed; we would prefer (48b) in these cases. The same method as employed in (48b), $\mathcal{H}^\Lambda_a[(\bullet^n f^{(n)}(\bullet))'] = \frac{1}{a}\mathcal{H}^\Lambda_a[((a-\bullet)+\bullet)(\bullet^n f^{(n)}(\bullet))']$, leads to the following generalisation of (48b):

$$\frac{d}{da}\Big(\frac{1}{a^n}\mathcal{H}^\Lambda_a[\bullet^n f^{(n)}(\bullet)]\Big) = -\frac{(\Lambda^2)^n f^{(n)}(\Lambda^2)}{\pi a^{n+1}(1-\frac{a}{\Lambda^2})} + \frac{1}{a^{n+1}}\mathcal{H}^\Lambda_a[\bullet^{n+1} f^{(n+1)}(\bullet)]\;.$$

Homogeneous contribution of $f^{(k)}(\Lambda^2)$ are then collected to

$$\frac{d^n}{da^n}\mathcal{H}^\Lambda_a[f(\bullet)] = \frac{1}{a^n}\mathcal{H}^\Lambda_a[\bullet^n f^{(n)}(\bullet)] + \frac{(-1)^n(n-1)!}{\pi a^n}\sum_{k=0}^{n-1}\frac{(-\Lambda^2)^k f^{(k)}(\Lambda^2)}{k!}F^\Lambda_{n,k}(a)\;, \qquad (49a)$$

$$F^\Lambda_{n,k}(a) := \frac{1}{(1-\frac{a}{\Lambda^2})}\sum_{p=0}^{n-k-1}\frac{\binom{n-k-1}{p}}{\binom{n-1}{p}}\Big(\frac{-a}{\Lambda^2-a}\Big)^p\;. \qquad (49b)$$

Alternatively, we can use (48a) for the first derivative and (49a) for higher derivatives:

$$\begin{aligned}\frac{d^n}{da^n}\mathcal{H}^\Lambda_a[f(\bullet)] &= \frac{(-1)^n(n-1)!}{\pi a^n}f(0) - \frac{(n-1)!}{\pi(\Lambda^2-a)^n}f(\Lambda^2) + \frac{1}{a^{n-1}}\mathcal{H}^\Lambda_a[\bullet^{n-1}f^{(n)}(\bullet)]\\ &\quad + \frac{(-1)^n(n-2)!}{\pi a^{n-1}\Lambda^2}\sum_{k=1}^{n-1}k\frac{(-\Lambda^2)^k f^{(k)}(\Lambda^2)}{k!}F^\Lambda_{n-1,k-1}(a)\;. \qquad (49c)\end{aligned}$$

This version is particularly useful if $f(0) = 0$.

Next we provide an equation for derivatives of $\cot\tau_b(a)$ with respect to a. In a first step we need

$$\begin{aligned}\Gamma_s(a) := \frac{(-1)^s a^s G_{a0}}{s!}\frac{d^s}{da^s}\frac{1}{G_{a0}} &= \sum_{l=0}^{s}\frac{(-1)^l l!}{s!}Y_{s,l}\Big(\Big\{\frac{(-a)^j G^{(j)}_{a0}}{G_{a0}}\Big\}_{j=1}^{s-l+1}\Big)\\ &= \sum_{l=0}^{s}\frac{(-1)^l}{s!}Y_{s,l}\Big(\big\{(-a)^j(\log G_{a0})^{(j)}\big\}_{j=1}^{s-l+1}\Big)\;. \qquad (50)\end{aligned}$$

Using (49a) we obtain for the derivatives of $\cot\tau_b(a)$ the formula

$$C_b^n(a) := (-1)^n|\lambda|\pi a^{n+1}\frac{d^n\cot\tau_b(a)}{da^n} = (-1)^n a^{n+1}\frac{d^n}{da^n}\Big(\frac{b}{a}+\frac{1}{G_{a0}}\Big(\frac{1}{a}+\lambda\pi\mathcal{H}_a^\Lambda[G_{\bullet 0}]\Big)\Big)$$
$$= n!\Bigg\{b+\frac{1+\lambda\pi a\mathcal{H}_a^\Lambda[G_{\bullet 0}]}{G_{a0}}\Gamma_n(a)$$
$$+\sum_{k=1}^{n}\frac{1+\frac{\lambda a}{k}\sum_{l=0}^{k-1}\frac{(-\Lambda^2)^l G^{(l)}_{0\Lambda^2}}{l!}F^\Lambda_{k,l}(a)+\lambda\pi a\mathcal{H}_a^\Lambda\big[\frac{(-\bullet)^k}{k!}G^{(k)}_{\bullet 0}\big]}{G_{a0}}\Gamma_{n-k}(a)\Bigg\}. \qquad (51)$$

We prefer here (49a) to (49c) because the latter leads to Hilbert transforms $\lambda\pi a^2\mathcal{H}_a^\Lambda\big[\frac{(-\bullet)^{k-1}}{k!}G^{(k)}_{\bullet 0}\big]$ instead of $\lambda\pi a\mathcal{H}_a^\Lambda\big[\frac{(-\bullet)^k}{k!}G^{(k)}_{\bullet 0}\big]$. Although both results must agree, the increased exponent $\lambda\pi a^2$ compared with $\lambda\pi a$ might lead in numerical simulations to larger errors[2].

According to (44a) and (49), a-derivatives of $\frac{\partial^\ell\log G_{ab}}{\partial b^\ell}$ involve the functions

$$A^{(n,\ell)}(a,b) := \frac{(-a)^n}{n!}\frac{(-b)^\ell}{\ell!}\frac{\partial^{n+\ell}A[\cot\tau_b(a)]}{\partial a^n\,\partial^\ell b} = \frac{(-a)^n}{n!}\frac{(-b)^\ell}{\ell!}\frac{\partial^n}{\partial a^n}\Big(\frac{A^{(\ell)}(\cot\tau_b(a))}{(|\lambda|\pi a)^\ell}\Big)$$
$$= \frac{(-a)^n}{n!}\frac{(-b)^\ell}{\ell!}\sum_{m=0}^{n}\binom{n}{m}\frac{\partial^m A^{(\ell)}[\cot\tau_b(a)]}{\partial a^m}\frac{(-1)^{n-m}(\ell+n-m-1)!}{(\ell-1)!(|\lambda|\pi)^\ell a^{\ell+n-m}}$$
$$= \sum_{m=0}^{n}\binom{n-m+\ell-1}{\ell-1}\sum_{k=0}^{m}\frac{(-a)^m}{m!\ell!}A^{(\ell+k)}[\cot\tau_b(a)]Y_{m,k}\Big(\Big\{\frac{(-1)^\kappa C_b^\kappa(a)}{|\lambda|\pi a^{\kappa+1}}\Big\}_{\kappa=1}^{m-k+1}\Big)\cdot\Big(\frac{-b}{|\lambda|\pi a}\Big)^\ell$$
$$= \sum_{m=0}^{n}\sum_{k=0}^{m}\binom{n-m+\ell-1}{\ell-1}\frac{(-1)^k(\ell+k)!}{m!\ell!}\frac{\sin((\ell+k)\tau_b(a))}{(\ell+k)}$$
$$\times\Big(\frac{b\sin\tau_b(a)}{|\lambda|\pi a}\Big)^\ell Y_{m,k}\Big(\Big\{\frac{C_b^\kappa(a)\sin\tau_b(a)}{|\lambda|\pi a}\Big\}_{\kappa=1}^{m-k+1}\Big). \qquad (52a)$$

In the third line Faà di Bruno and the definition (51) have been used. To obtain the last equation we have reinserted Lemma 5 and used the homogeneity properties of the Bell polynomials. For $m\geq 1$ the second sum actually restricts to $k\geq 1$. Formula (52a) extends to the case (n=0, $\ell\geq$1) where it reproduces $\frac{(-b)^\ell}{\ell!}$ times the function under the Hilbert transform in (44b). For ($n\geq$1, ℓ=0) only the terms with $m=n$ survive (which forces $k\geq 1$), and (n=0, ℓ=0) is easily included:

$$A^{(n,0)}(a,b) := \frac{(-a)^n}{n!}\frac{\partial^n A[\cot\tau_b(a)]}{\partial a^n}$$

[2] At this point a remark on the limit $\Lambda^2\to\infty$ is in order. Of course $\lim_{\Lambda^2\to\infty}\cot\tau_b(a)$ is expected to exist, and its derivatives should reproduce the limit $\Lambda^2\to\infty$ of (51) as a whole. But there is no reason to assume that all individual terms in (51) converge for $\Lambda^2\to\infty$.

$$= \begin{cases} \tau_b(a) & \text{for } n = 0 \,, \\ \displaystyle\sum_{k=1}^{n} \frac{(-1)^k k!}{n!} \frac{\sin(k\tau_b(a))}{k} Y_{n,k}\Big(\Big\{ \frac{C_b^\kappa(a) \sin \tau_b(a)}{|\lambda|\pi a} \Big\}_{\kappa=1}^{n-k+1} \Big) & \text{for } n \geq 1 \,. \end{cases} \tag{52b}$$

In complete analogy one finds for $\ell \geq 1$ and any n

$$\begin{aligned} L^{(n,\ell)}(a,b) &:= \frac{(-a)^n}{n!} \frac{(-b)^\ell}{\ell!} \frac{\partial^{n+\ell}}{\partial a^n \, \partial^\ell b} \Big(L[\cot \tau_b(a)] - \log(|\lambda|\pi a) \Big) \\ &= \sum_{m=0}^{n} \sum_{k=0}^{m} \binom{n-m+\ell-1}{\ell-1} \frac{(-1)^k (\ell+k)!}{m! \ell!} \frac{\cos((\ell+k)\tau_b(a))}{(\ell+k)} \\ &\qquad \times \Big(\frac{b \sin \tau_b(a)}{|\lambda|\pi a} \Big)^\ell Y_{m,k}\Big(\Big\{ \frac{C_b^\kappa(a) \sin \tau_b(a)}{|\lambda|\pi a} \Big\}_{\kappa=1}^{m-k+1} \Big) \,, \end{aligned} \tag{53a}$$

whereas for $\ell = 0$, $n \geq 1$ one has

$$\begin{aligned} L^{(n,0)}(a,b) &:= \frac{(-a)^n}{n!} \frac{\partial^n}{\partial a^n} \Big(L[\cot \tau_b(a)] - \log(|\lambda|\pi a) \Big) \\ &= \frac{1}{n} + \sum_{k=1}^{n} \frac{(-1)^k k!}{n!} \frac{\cos(k\tau_b(a))}{k} Y_{n,k}\Big(\Big\{ \frac{C_b^\kappa(a) \sin \tau_b(a)}{|\lambda|\pi a} \Big\}_{\kappa=1}^{n-k+1} \Big) \,. \end{aligned} \tag{53b}$$

These formulae are inserted into the a-derivatives of (44a), however with a smaller cut-off $\Lambda \mapsto \tilde{\Lambda} < \Lambda$. The reason is the singularity of $C_b^n(a)$ at $a = \Lambda^2$, which excludes the values at Λ^2 in (49c). Since we have $A^{(n,\ell)}(0,b) = 0$, we can use (48a) for $n = 1$ and (49c) for $n \geq 2$ to obtain:

$$\begin{aligned} &\frac{(-a)^n}{n!} \frac{(-b)^\ell}{\ell!} \frac{\partial^{n+\ell} \log G_{ab}}{\partial a^n \partial b^\ell}\Big|_{n\geq 1} \\ &\quad = \lambda\pi a \, \mathcal{H}_a^{\tilde{\Lambda}} \Big[\frac{A^{(n,\ell)}(\bullet, b)}{|\lambda|\pi \bullet} \Big] + L^{(n,\ell)}(a,b) - \frac{\operatorname{sign}(\lambda)}{n\pi} \Big(\frac{-a}{\tilde{\Lambda}^2 - a} \Big)^n A^{(0,\ell)}(\tilde{\Lambda}^2, b) \\ &\qquad + \begin{cases} \dfrac{\operatorname{sign}(\lambda)}{\pi n(n-1)} \dfrac{a}{\tilde{\Lambda}^2} \displaystyle\sum_{k=1}^{n-1} k A^{(k,\ell)}(\tilde{\Lambda}^2, b) \, F_{n-1,k-1}^{\tilde{\Lambda}}(a) & \text{for } n \geq 2 \,, \\ 0 & \text{for } n = 1 \,. \end{cases} \end{aligned} \tag{54}$$

We prefer here (49c) to (49a) in order to make explicit that (54) vanishes for $a = 0$. We only rely on cancellations giving $L^{(n,\ell)}(0,b) = 0$ (we prove this in Appendix B, together with the related computation of $\lim_{a\to 0} \frac{A^{(n,\ell)}(a,b)}{|\lambda|\pi a}$) but not on cancellations under the Hilbert transform which numerically are not guaranteed. We thus conclude that Widder's operators $L_{n,t}[G_{\bullet\bullet}]$ defined by (36) vanish at $t = 0$. Finally we remark that the case $\ell = 0$ of (54) should be the symmetric partner to (44b). This would imply that $\frac{(-a)^n}{n!} \frac{(-b)^\ell}{\ell!} \frac{\partial^{n+\ell} \log G_{ab}}{\partial a^n \partial b^\ell}$ vanishes to n^{th} order in $a = 0$. The proof relies on subtle cancellations which cannot be expected for the numerical result.

We have thus established:

Proposition 6 *For natural numbers $s \geq 2, h \geq 1$ one has*

$$L_{s,a}[G_{\bullet\bullet}] = \sum_{l=0}^{s} \frac{(-1)^{s-l}(2s-1)!}{(2s-l-1)!(s-2)!(s-l)!l!} \cdot (-a)^{2s-l-1} G_{aa}^{(2s-l-1)} \,, \tag{55a}$$

$$(-a)^h G_{aa}^{(h)} = G_{aa} \sum_{k=0}^{h} Y_{h,k}\big(\{(-a)^n (\log G_{aa})^{(n)}\}_{n=1}^{h-k+1}\big) \,. \tag{55b}$$

The occurring functions $(-a)^n(\log G_{aa})^{(n)}$, for $n \geq 1$, are given in terms of $A^{(n,\ell)}, L^{(n,\ell)}$ defined in (52)+(53), which rely on $\tau_b(a)$ defined in (14), $C_b^\kappa(a)$ defined in (51), $\Gamma_l(a)$ defined in (50) and $F_{n,k}^\Lambda(a)$ defined in (49b), by

$$\begin{aligned}
&(-a)^n(\log G_{aa})^{(n)} \\
&= n!\Big\{ \operatorname{sign}(\lambda)\, \mathcal{H}_a^{\tilde\Lambda}\big[A^{(0,n)}(\bullet, a)\big] + L^{(0,n)}(a,a) \\
&+ \sum_{\ell=0}^{n-1} \Big\{ \lambda\pi a \mathcal{H}_a^{\tilde\Lambda}\Big[\frac{A^{(n-\ell,\ell)}(\bullet,a)}{|\lambda|\pi\bullet}\Big] + L^{(n-\ell,\ell)}(a,a) - \frac{\operatorname{sign}(\lambda)\, A^{(0,\ell)}(\tilde\Lambda^2, a)}{\pi(n-\ell)} \Big(\frac{-a}{\tilde\Lambda^2 - a}\Big)^{n-\ell} \Big\} \\
&\quad + \sum_{\ell=0}^{n-2} \sum_{k=1}^{n-\ell-1} \frac{\operatorname{sign}(\lambda)}{\pi(n-\ell)(n-\ell-1)} \Big(\frac{a}{\tilde\Lambda^2}\Big)\, k A^{(k,\ell)}(\tilde\Lambda^2, a)\, F_{n-\ell-1,k-1}^{\tilde\Lambda}(a) \Big\}.
\end{aligned} \tag{55c}$$

In this way, $L_{s,a}[G_{\bullet\bullet}]$ is eventually expressed in terms of G_{a0} and its derivatives, which under use of $G_{a0} = G_{0a}$ are given by (32) and its derivatives (45).

Proof. (55a) is an obvious rewriting of (36), and (55b) is Faà di Bruno applied to $G_{aa} = \exp(\log(G_{aa}))$ together with homogeneity properties of the Bell polynomials (42). Finally, (55c) follows from (40) taken at $b \mapsto a$ together with (54) and insertion of (52) and (53). □

4 Numerical results

We use the computer algebra system *Mathematica*^{TM} for a numerical approximation of the two-point function. We need no sophisticated tools of *Mathematica*^{TM}; everything boils down to standard manipulations of arrays and basic mathematical functions $\exp, \log, \sqrt{}, \arctan, \sin, \cos, +, -, \times, \div$. We provide in Appendix A the source code, together with additional explanations, of our implementation so that the reader can check and adapt our calculation or reimplement it in other computer languages. We do not claim that our code is optimal, and we do not provide any error handling.

In this section we summarise the main results of this numerical implementation:

1. The fixed point equation (32) satisfies (numerically) the assumptions of the Banach fixed point theorem for any $\lambda \in \mathbb{R}$. We can thus compute G_{0b} and hence, in principle, all correlation functions and Widder's operators $L_{n,t}[G_{\bullet\bullet}]$ with sufficient precision.

2. For $\lambda > 0$, neglecting C_{λ,Λ^2} and f_{λ,Λ^2} in (18) is *not justified*. At the moment we see no possibility to improve this situation for $\lambda > 0$.
3. For $\lambda < 0$ everything is consistent within small numerical error bounds. The symmetry $G_{ab} = G_{ba}$ is confirmed. The derivative $\frac{d\mathcal{Y}}{d\lambda}$ of the finite wavefunction renormalisation $\mathcal{Y} = \mathcal{Y}_1$ is discontinuous at some critical (negative) coupling constant $\lambda_c \approx -0.39$, which we interpret as a phase transition at λ_c. Whereas the phase $\lambda_c < \lambda \leq 0$ has good properties, we have $\mathcal{Y} = -1$ within small error bounds for $\lambda < \lambda_c$. This implies that higher correlation functions loose their meaning in the phase $\lambda < \lambda_c$.
4. The Stieltjes property of the diagonal 2-point function, equivalent to reflection positivity of the Schwinger 2-point function [10], is excluded *outside* the window $[\lambda_c, 0]$. We have good reasons to assume that the Stieltjes property holds for $\lambda_c < \lambda \leq 0$, but this needs further verification.

4.1 Convergence of the iteration for $\lambda = \frac{1}{\pi}$

The fixed point equation (32) defines an operator $\tilde{T} := \exp \circ T \circ \log$ via $G_{0b} = (\tilde{T}G)(b)$. We have shown in [14] that $T : \mathcal{K}_\lambda \to \mathcal{K}_\lambda$ satisfies for $-\frac{1}{6} \leq \lambda \leq 0$ the assumptions of the Schauder fixed point theorem. In addition, $(\tilde{T}1)(b) = 1$ for any $\lambda < 0$ [14, Appendix A]. For $\lambda > 0$ we have already seen in [6] that $\tilde{T}$ has a fixed point by the Schauder fixed point theorem.

Here we test numerically the conjecture that $\tilde{T}$ also satisfies the assumptions of the Banach fixed point theorem. This would imply that starting from an arbitrary initial function $G^0 \in \mathcal{K}$ in a closed subset of a Banach space, the iteration $G^{i+1} := \tilde{T}G^i$ converges to the fixed point solution $G = \tilde{T}G = \lim_{i\to\infty} G^i$. It would be most natural to take the Banach space $\mathcal{C}^1_0(\mathbb{R}^+)$ of differentiable functions vanishing at ∞ as in [6]. A good numerical substitute is the Banach space $\mathcal{C}^{0,1}([0,\Lambda^2])$ of Lipschitz continuous functions on $[0,\Lambda^2]$. We approximate G_{0b} by a piecewise linear function (which is Lipschitz) determined by its corner values at $L+1$ sample points $0 = b_1 < b_2 \cdots < b_L < b_{L+1} = \Lambda^2$. After initialisation of these sample points in[3] **In[7]** we compute the corner values of G_{0b} by an iteration **In[8]**.

In table 1 we study for $\lambda = \frac{1}{\pi}$ the dependence **In[7]** of G_{0b} and G_{aa} on the parameters $\Lambda^2 =$ `co`, $L =$ `len` and `infty` of the *Mathematica*^{TM}-implementation. Typical numerical results for `len=10^4`, `co=10^7` are visualised in fig. 1. We observe:

- The convergence of the iteration $G^{\mathtt{i}} \mapsto G^{\mathtt{i+1}}$ in Lipschitz norm $\|f\| = \sup_{0\leq a\leq\Lambda^2} |f(a)| + \sup_{0\leq a<b\leq\Lambda^2} \left|\frac{f(a)-f(b)}{a-b}\right|$ is remarkably good for any cutoff `co`$=\Lambda^2$. Each iteration step reduces the norm error by a factor bigger than 2.
- If the cut-off `co`$=\Lambda^2$ is too small, then the absolute asymmetry `AbsAsm` $= \sup_{0\leq a<b<\Lambda^2} |G_{ab} - G_{ba}|$ is governed by boundary effects at $b \approx \Lambda^2$. For larger cut-off the largest asymmetry is located where $a, b \approx 0$ because G_{ab} is largest there.

[3] **In[...]** refers to the implementation in Appendix A.

Approximation $G^{\mathtt{i}}$ for G_{0b} at $\lambda = \frac{1}{\pi}$, $\mathtt{i} = 20$ iterations of $G^0_{0b} = 1$								
co	len	∞	$G^{\mathtt{i}}_{0,100}$	$G^{\mathtt{i}}_{0,\mathtt{co}}$	$\|G^{\mathtt{i}} - G^{\mathtt{i-1}}\|$	AbsAsm	$A + Bx$	$C + Dx$
10^2	10^3	10^8	0.0027095	2.7×10^{-3}	1.9×10^{-11}	2.7×10^{-3}	$0.030-1.290x$	$-0.344-1.351x$
10^3	10^3	10^8	0.0023612	1.1×10^{-4}	1.7×10^{-9}	1.4×10^{-4}	$0.085-1.330x$	$-0.365-1.341x$
10^4	10^3	10^8	0.0023225	4.2×10^{-6}	6.6×10^{-9}	4.6×10^{-5}	$0.148-1.358x$	$-0.340-1.353x$
10^5	10^3	10^8	0.0023180	1.5×10^{-7}	1.0×10^{-8}	7.1×10^{-5}	$0.211-1.379x$	$-0.293-1.368x$
10^5	10^3	$\mathbf{10^9}$	0.0023180	1.5×10^{-7}	1.0×10^{-8}	7.1×10^{-5}	$0.211-1.379x$	$-0.293-1.368x$
10^6	10^3	10^9	0.0023174	5.5×10^{-9}	1.2×10^{-8}	9.7×10^{-5}	$0.272-1.395x$	$-0.239-1.382x$
10^6	10^4	10^9	0.0023177	5.5×10^{-9}	1.2×10^{-8}	$\mathbf{1.7\times10^{-6}}$	$0.272-1.395x$	$-0.226-1.384x$
10^7	10^3	10^{10}	0.0023173	2.0×10^{-10}	1.3×10^{-8}	1.3×10^{-4}	$0.318-1.405x$	$-0.196-1.391x$
10^7	$\mathbf{10^4}$	10^{10}	0.0023176	2.2×10^{-10}	1.3×10^{-8}	$\mathbf{2.2\times10^{-6}}$	$0.304-1.402x$	$-0.168-1.396x$
10^8	10^3	10^{12}	0.0023172	1.2×10^{-11}	1.3×10^{-8}	1.6×10^{-4}	$0.277-1.398x$	$-0.172-1.455x$
10^8	$\mathbf{10^4}$	10^{12}	0.0023172	1.2×10^{-11}	1.4×10^{-8}	$\mathbf{2.8\times10^{-6}}$	$0.244-1.392x$	$-0.769-1.557x$

Table 1: The 2-point function G_{0b} at $\lambda = \frac{1}{\pi}$ for various cut-offs co and resolutions len.

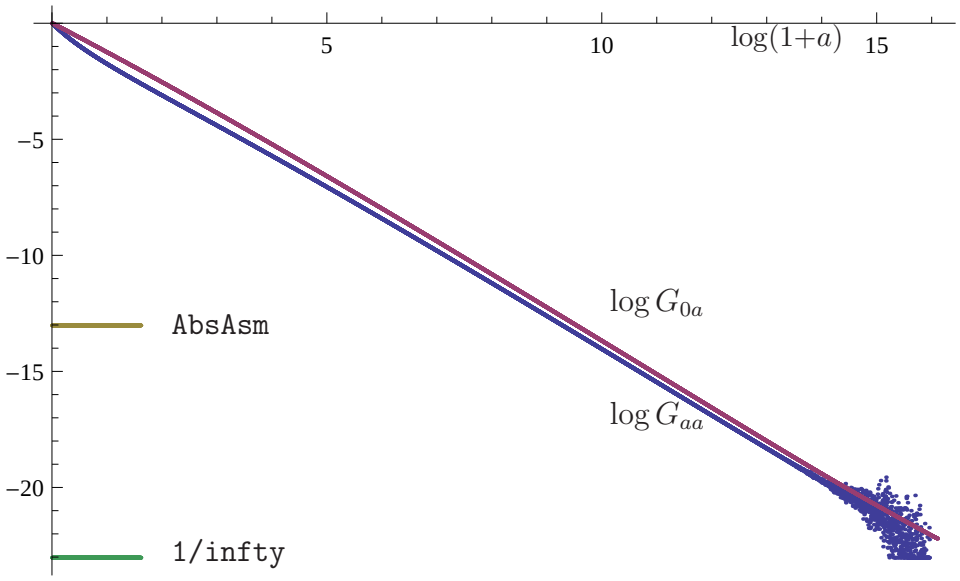

Figure 1: Plot of the logarithm of the boundary and diagonal 2-point functions G_{0a} (red, upper curve) and G_{aa} (blue, lower curve) over $\log(1+a)$, for $\lambda = \frac{1}{\pi}$ in numerical approximation i=20, co=10^7, len=10^4. The noise in G_{aa} appears near 1/infty, hence much beyond the asymmetry AbsAsm.

The asymmetry is reduced if more sample points (increased len=L, see len=10^4 versus len=10^3 at co=10^7) are included. The computation time of our algorithm grows at least quadratically in len. The relative asymmetry turns out large near the boundary. We address this problem in sec. 4.2.

- The numerical choice of `infty` for $\infty = \lim_{\epsilon\to 0} \log \frac{a_2-a_1}{\epsilon}$ has no influence. For `co`=10^5, `len`=10^3 the sup-norm difference $\sup_a |G_{0a}^{\texttt{infty}=10^8} - G_{0a}^{\texttt{infty}=10^9}|$ is of the order 10^{-14}. We nevertheless keep `1/infty` of the same order as $G_{0,\texttt{co}}$.
- The cut-off 2-point function $G_{0a}(\Lambda^2)$ is pointwise convergent for $\Lambda \to \infty$.
- Previous numerical simulations in the preprint arXiv:1205.0465v1 of [6] had suggested an asymptotic behaviour $G_{0a} \propto \frac{1}{(1+a)^{1+\lambda}}$, i.e. $\log G_{0a} \propto -(1+\lambda)\log(1+a)$ is linear. The corresponding fits of $\log G_{0,\exp(x)-1}$ to a line $A + Bx$ and of $\log G_{\exp(x)-1,\exp(x)-1}$ to a line $C + Dx$ are also indicated in table 1. We thus confirm that the slope actually decreases with the cut-off without any hint of convergence.
- As shown in fig. 1 there is clear evidence that G_{0a} and G_{aa} have the same asymptotic behaviour for $a \to \infty$. The previously conjectured asymptotics holds without any doubt in form of inequalities

$$0 < G_{0a} < \frac{C}{(1+a)^{1+\lambda}}\,, \qquad 0 < G_{aa} < \frac{C'}{(1+a)^{1+\lambda}}\,.$$

  This is enough to state that the function $a \mapsto G_{aa}$ is for $\lambda > 0$ not a Stieltjes function. The results of [10] then imply that the corresponding Euclidean quantum field theory does not have an analytic continuation to a Wightman theory for $\lambda > 0$.

4.2 Varying $\lambda > 0$: Inconsistency

Next we study the dependence of G_{0b} and G_{aa} on $\lambda \geq 0$. The convergence rate of the iteration `i`→`i+1` is highly sensitive to λ. To have comparable results we run the iteration until $G^{\texttt{i}}$ and $G^{\texttt{i}-1}$ differ by $< 4\times 10^{-8}$ in supremum norm. This is achieved by replacing in the `For[ ]`-loop of **In[8]** the termination condition `If[i>=20, Break[]];` by

```
If[SupNorm[gs[i], gs[i-1]] < 4*10^(-8), Break[]];
```

The results are given in table 2. We notice a sudden increase of the absolute asymmetry $\texttt{AbsAsm} = \sup_{0\leq a<b\leq\Lambda^2} |G_{ab}-G_{ba}|$ for $\lambda > \frac{1.1}{\pi}$ which goes hand in hand with qualitative change of the function $a \mapsto G_{aa}$: Whereas for $0 \leq \lambda < \frac{1.05}{\pi}$ the slopes B, C are comparable, we find for $\lambda > \frac{1.1}{\pi}$ that D grows much faster than B and stabilises at $D \approx B+1$ for $\lambda > \frac{2}{\pi}$. A look at the relative asymmetry $\texttt{RelAsm} = \sup_{0\leq a<b<\Lambda^2} \frac{|G_{ab}-G_{ba}|}{G_{ab}+G_{ba}}$ shows, however, that the true transition already occurs at[4] $\lambda \approx \frac{0.7}{\pi}$. We show on the left of fig. 2 the absolute and relative asymmetry in a logarithmic scale and on the right of fig. 2 the relative asymmetry in a linear scale, including the results for $\lambda < 0$ obtained in sec. 4.3. The plot of the relative asymmetry identifies three clearly different regions in λ: For $\lambda < 0$ the function G_{ab} is symmetric up to small discretisation errors of a few percent. For $0 < \lambda < \frac{0.7}{\pi}$ we have

[4] Interestingly, this value coincides with slowest convergence of the iteration. The phase transition at $\lambda_c \approx -\frac{1.24}{\pi}$ identified in the next subsection also coincides with slowest convergence rate for $\lambda < 0$. A possible origin is a change of sign of Z for finite Λ, see (26).

Approximation $G^{\mathtt{i}}$ as function of λ, with $\sup_b \lvert G^{\mathtt{i}}_{0b} - G^{\mathtt{i}-1}_{0b}\rvert < 4{\times}10^{-8}$ `co=10^7`, `len=2000`, `infty=10^(10)`								
$\lambda\pi$	i	$G^{\mathtt{i}}_{\mathtt{co},0}$	AbsAsm	RelAsm	$A + Bx$	$C + Dx$	$\mathcal{Y}$	$\lambda_{\mathit{eff}}\pi$
3.0	7	$1.0{\times}10^{-11}$	$1.0{\times}10^{-1}$	1.0000	$0.433{-}1.588x$	$1.47{-}2.595x$	0.340	3.117
2.5	7	$1.1{\times}10^{-11}$	$6.5{\times}10^{-2}$	1.0000	$0.446{-}1.587x$	$1.87{-}2.571x$	0.334	2.613
2.0	7	$1.1{\times}10^{-11}$	$3.0{\times}10^{-2}$	1.0000	$0.473{-}1.583x$	$2.35{-}2.520x$	0.322	2.107
1.8	7	$1.2{\times}10^{-11}$	$1.8{\times}10^{-2}$	1.0000	$0.492{-}1.580x$	$2.57{-}2.482x$	0.314	1.904
1.6	8	$1.3{\times}10^{-11}$	$8.6{\times}10^{-3}$	1.0000	$0.518{-}1.575x$	$2.76{-}2.420x$	0.303	1.700
1.4	9	$1.5{\times}10^{-11}$	$2.6{\times}10^{-3}$	1.0000	$0.556{-}1.566x$	$2.85{-}2.304x$	0.288	1.494
1.3	9	$1.7{\times}10^{-11}$	$9.6{\times}10^{-4}$	1.0000	$0.580{-}1.558x$	$2.75{-}2.198x$	0.279	1.389
1.2	11	$2.1{\times}10^{-11}$	$1.9{\times}10^{-4}$	1.0000	$0.603{-}1.544x$	$2.34{-}2.017x$	0.267	1.282
1.15	11	$2.5{\times}10^{-11}$	$4.6{\times}10^{-5}$	1.0000	$0.608{-}1.531x$	$1.86{-}1.868x$	0.261	1.228
1.1	12	$3.3{\times}10^{-11}$	$4.3{\times}10^{-5}$	0.9999	$0.594{-}1.511x$	$0.99{-}1.649x$	0.254	1.171
1.05	14	$8.5{\times}10^{-11}$	$4.1{\times}10^{-5}$	0.9990	$0.474{-}1.462x$	$0.006{-}1.443x$	0.246	1.113
1.0	18	$2.1{\times}10^{-10}$	$3.8{\times}10^{-5}$	0.9906	$0.313{-}1.404x$	$-0.188{-}1.392x$	0.238	1.055
0.95	25	$3.7{\times}10^{-10}$	$3.5{\times}10^{-5}$	0.9667	$0.235{-}1.365x$	$-0.274{-}1.360x$	0.229	0.997
0.9	36	$5.7{\times}10^{-10}$	$3.3{\times}10^{-5}$	0.9231	$0.189{-}1.335x$	$-0.329{-}1.333x$	0.220	0.940
0.8	58	$1.2{\times}10^{-9}$	$2.8{\times}10^{-5}$	0.7864	$0.124{-}1.284x$	$-0.403{-}1.288x$	0.202	0.828
0.7	57	$2.4{\times}10^{-9}$	$2.3{\times}10^{-5}$	0.6396	$0.081{-}1.240x$	$-0.455{-}1.247x$	0.182	0.719
0.6	42	$4.4{\times}10^{-9}$	$1.8{\times}10^{-5}$	0.3825	$0.053{-}1.200x$	$-0.493{-}1.209x$	0.160	0.612
0.5	29	$7.8{\times}10^{-9}$	$1.4{\times}10^{-5}$	0.3892	$0.032{-}1.164x$	$-0.521{-}1.174x$	0.137	0.507
0.4	20	$1.3{\times}10^{-8}$	$1.1{\times}10^{-5}$	0.4038	$0.017{-}1.129x$	$-0.541{-}1.140x$	0.113	0.404
0.3	13	$2.2{\times}10^{-8}$	$7.3{\times}10^{-6}$	0.4240	$0.007{-}1.095x$	$-0.554{-}1.107x$	0.087	0.303
0.2	10	$3.7{\times}10^{-8}$	$4.5{\times}10^{-6}$	0.4371	$0.001{-}1.063x$	$-0.560{-}1.075x$	0.060	0.200
0.1	8	$6.1{\times}10^{-8}$	$2.0{\times}10^{-6}$	0.4491	$-0.001{-}1.031x$	$-0.562{-}1.043x$	0.031	0.100
0.05	7	$7.8{\times}10^{-8}$	$9.5{\times}10^{-7}$	0.4546	$-0.001{-}1.016x$	$-0.561{-}1.028x$	0.016	0.050
0.0	2	$1.0{\times}10^{-7}$	0	0	$0.000{-}1.000x$	$-0.558{-}1.012x$	0	0

Table 2: Fixed point solution G_{0a} of (32) for $\lambda \geq 0$

some 40% asymmetry, whereas for larger λ the asymmetry strongly increases to nearly 100% for $\lambda > \frac{1}{\pi}$.

The region of $\lambda > \frac{1}{\pi}$ where the relative asymmetry nearly reaches 100% also shows a qualitative change of the function $a \mapsto G_{aa}$. As shown in fig. 3, there is a critical a where the slope of $\log(1+a) \mapsto \log G_{aa}$ suddenly decreases by 1. This critical a gets larger for smaller λ. It is near the cut-off `co`$=10^7$ for $\lambda = \frac{1}{\pi}$ and moves into $[0, 10^7]$ for larger λ. This observation lets us conjecture that *the entire region $\lambda > 0$ shows a critical value of a where the slope of* $\log(1+a) \mapsto \log G_{aa}$ *decreases by* 1. We tend to think that as λ increases from 0 to $\frac{1.0}{\pi}$, the decrease of slope becomes more and more visible and hence induces the jump of the relative asymmetry to nearly 100% in the region $\frac{0.6}{\pi} < \lambda < \frac{1.0}{\pi}$.

There remains this background relative asymmetry of $\approx 40\%$ which is not explained by

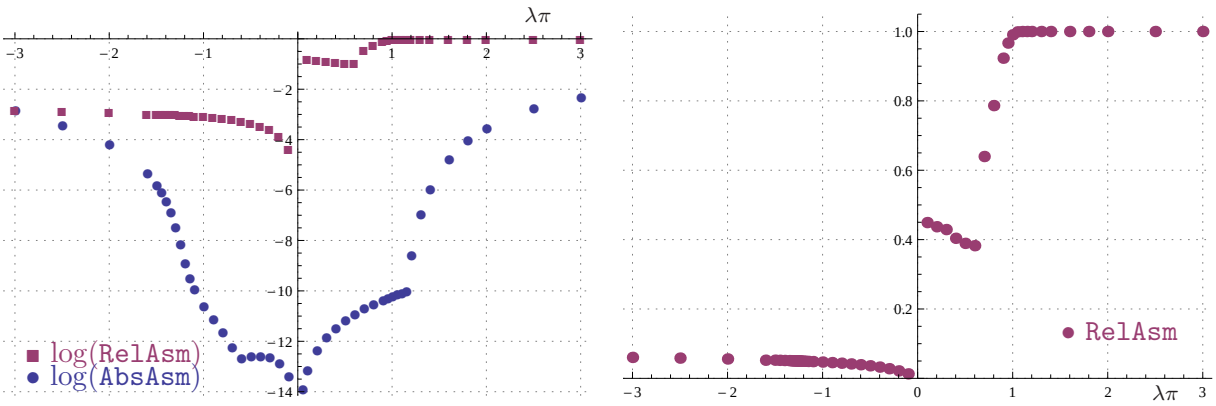

Figure 2: Left: Plot of the logarithms of absolute (blue dots) and relative (red squares) asymmetries as function of λ.
Right: Plot of the relative asymmetry as function of λ.

the decrease of slope. We trace this back to $f_{\lambda,\Lambda^2} \neq 0$ in (18) by the following investigation: The decreased slope by 1 is naturally interpreted as missing factor $1 + \frac{C_{\lambda,\Lambda^2}\Lambda^2 a}{\Lambda^2 - a}$. We derive in (33) the formula for C_{λ,Λ^2} under the assumption $f_{\lambda,\Lambda^2}(b) = 0$. This formula is implemented in **In[11]**. Necessary for validity of $f_{\lambda,\Lambda^2}(b) = 0$ is that `ClL[lis_, hilb_, xi_, a_]` is (up to numerical errors) independent of a. Typical results are shown in fig. 4. We notice that the function is approximately constant in a middle region $\exp(5) \approx 150 \leq a \leq \exp(14) \approx 1.2 \times 10^6$. For larger a the noise is too large, whereas for small a together with smaller λ there is a clear discrepancy. We see this as indication that *also the assumption* $f_{\lambda,\Lambda^2} = 0$ *is not justified for* $\lambda > 0$.

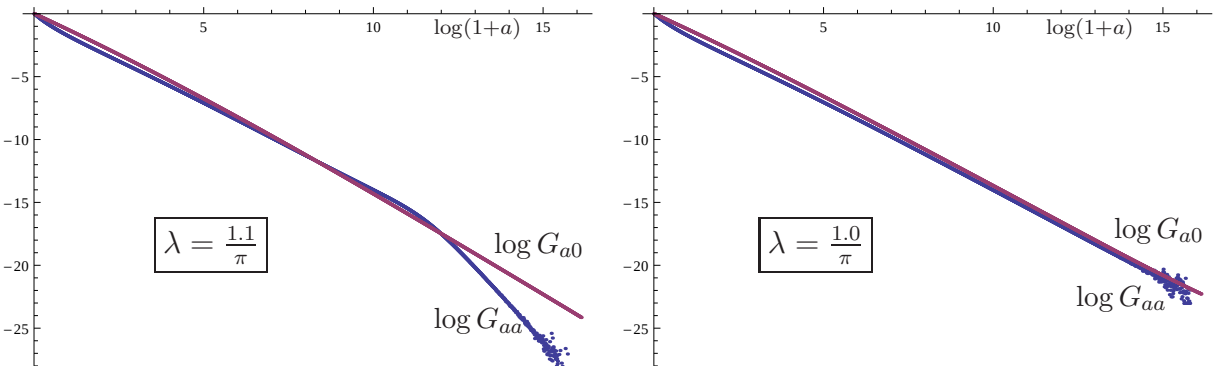

Figure 3: Comparison of the functions $\log G_{a0}$ (red) and $\log G_{aa}$ (blue) over $\log(1+a)$ for $\lambda = \frac{1.1}{\pi}$ (left) with $\lambda = \frac{1.0}{\pi}$ (right). The buckle in $\log G_{aa}$ for $\lambda = \frac{1.1}{\pi}$ moves to smaller a with increasing λ. At larger cut-off $\Lambda^2 = 10^8$ there is also a buckle for $\lambda = \frac{1.0}{\pi}$.

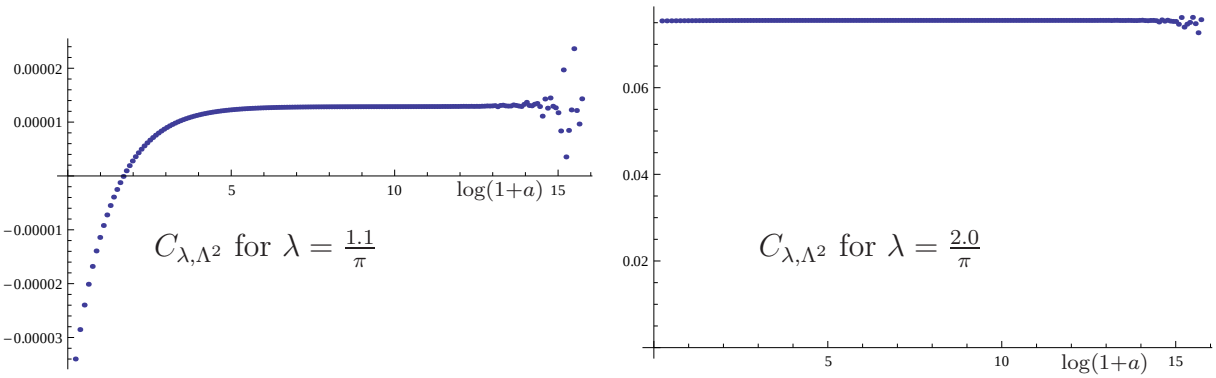

Figure 4: The parameter $C_{\lambda,\Lambda}$ plotted as numerical function of a. The result should be constant within numerical errors.

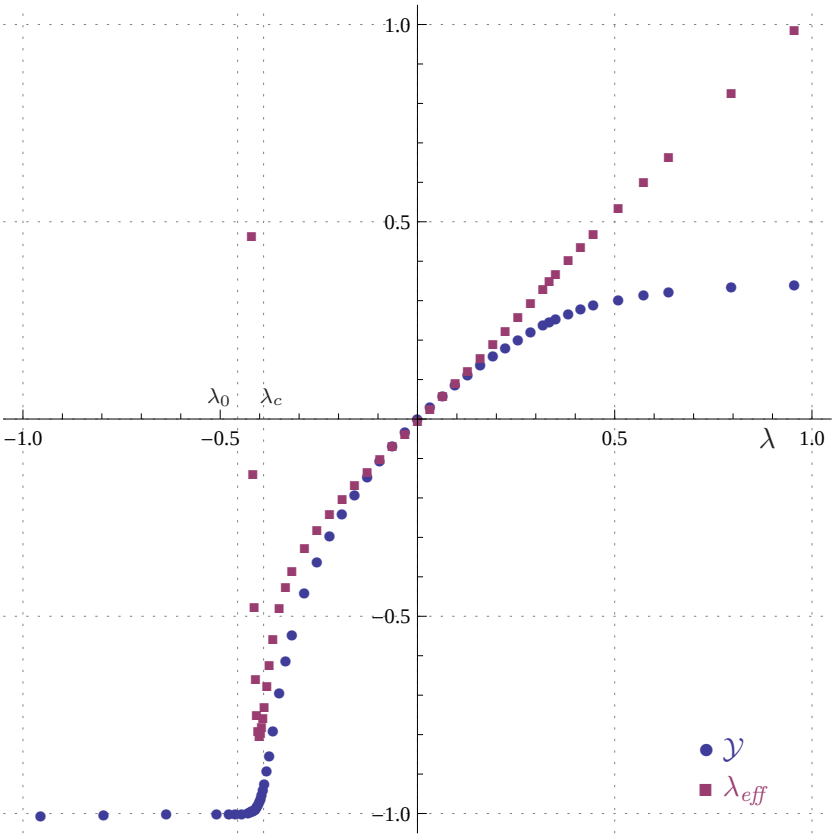

Figure 5: Plot of the finite wavefunction renormalisation $\mathcal{Y}$ (blue dots) and of the effective coupling constant λ_{eff} (red squares) as function of λ. The points $\lambda_0 \approx -\frac{1.432}{\pi}$ where $\mathcal{Y}(\lambda_0) = -1$ and $\lambda_c \approx -0.39$ where $\mathcal{Y}'(\lambda_c)$ is discontinuous are indicated as two of the dashed grid lines.

Approximation $G^{\mathtt{i}}$ as function of λ, with $\sup_b \lvert G^{\mathtt{i}}_{0b} - G^{\mathtt{i}-1}_{0b}\rvert < 4{\times}10^{-8}$ `co=10^7`, `len=2000`, `infty=10^(10)`							
$\lambda\pi$	i	$G^{\mathtt{i}}_{0,100}$	$G^{\mathtt{i}}_{0,\mathtt{co}}$	AbsAsm	RelAsm	$\mathcal{Y}$	$\lambda_{\mathit{eff}}\pi$
0.00	2	0.00990	$1.0{\times}10^{-7}$	0	0	0	0
−0.10	14	0.01149	$1.6{\times}10^{-7}$	$1.6{\times}10^{-6}$	0.0129	−0.0329	−0.100
−0.20	20	0.01339	$2.7{\times}10^{-7}$	$2.6{\times}10^{-6}$	0.0215	−0.0680	−0.201
−0.30	25	0.01569	$4.4{\times}10^{-7}$	$3.3{\times}10^{-6}$	0.0278	−0.1059	−0.302
−0.40	32	0.01854	$7.4{\times}10^{-7}$	$3.5{\times}10^{-6}$	0.0325	−0.1468	−0.405
−0.50	40	0.02213	$1.3{\times}10^{-6}$	$3.5{\times}10^{-6}$	0.0362	−0.1915	−0.511
−0.60	50	0.02678	$2.2{\times}10^{-6}$	$3.2{\times}10^{-6}$	0.0392	−0.2409	−0.621
−0.70	64	0.03305	$3.9{\times}10^{-6}$	$5.1{\times}10^{-6}$	0.0416	−0.2969	−0.737
−0.80	83	0.04199	$7.4{\times}10^{-6}$	$9.0{\times}10^{-6}$	0.0437	−0.3620	−0.864
−0.90	113	0.05582	$1.5{\times}10^{-5}$	$1.5{\times}10^{-5}$	0.0454	−0.4416	−1.009
−1.00	162	0.08016	$3.4{\times}10^{-5}$	$2.6{\times}10^{-5}$	0.0470	−0.5459	−1.196
−1.05	200	0.10071	$5.5{\times}10^{-5}$	$3.4{\times}10^{-5}$	0.0476	−0.6132	−1.321
−1.10	251	0.13275	$9.4{\times}10^{-5}$	$4.9{\times}10^{-5}$	0.0483	−0.6947	−1.490
−1.15	320	0.18679	$1.7{\times}10^{-4}$	$7.7{\times}10^{-5}$	0.0489	−0.7912	−1.737
−1.18	366	0.23790	$2.7{\times}10^{-4}$	$1.1{\times}10^{-4}$	0.0493	−0.8526	−1.943
−1.20	396	0.28352	$3.6{\times}10^{-4}$	$1.4{\times}10^{-4}$	0.0495	−0.8913	−2.106
−1.22	420	0.34038	$4.9{\times}10^{-4}$	$1.9{\times}10^{-4}$	0.0497	−0.9253	−2.279
−1.23	428	0.37323	$5.8{\times}10^{-4}$	$2.2{\times}10^{-4}$	0.0498	−0.9397	−2.361
−1.24	433	0.40886	$6.8{\times}10^{-4}$	$2.5{\times}10^{-4}$	0.0499	−0.9521	−2.434
−1.25	434	0.44695	$7.9{\times}10^{-4}$	$2.9{\times}10^{-4}$	0.0500	−0.9626	−2.487
−1.26	432	0.48697	$9.3{\times}10^{-4}$	$3.4{\times}10^{-4}$	0.0501	−0.9711	−2.506
−1.28	419	0.57004	$1.3{\times}10^{-3}$	$4.5{\times}10^{-4}$	0.0503	−0.9831	−2.341
−1.30	399	0.65194	$1.7{\times}10^{-3}$	$5.9{\times}10^{-4}$	0.0506	−0.9902	−1.480
−1.32	375	0.72699	$2.2{\times}10^{-3}$	$8.1{\times}10^{-4}$	0.0508	−0.9943	1.477
−1.35	340	0.81897	$3.1{\times}10^{-3}$	$1.0{\times}10^{-3}$	0.0511	−0.9974	21.37
−1.40	288	0.91426	$5.2{\times}10^{-3}$	$1.6{\times}10^{-3}$	0.0515	−0.9995	614.6
−1.45	248	0.95914	$7.9{\times}10^{-3}$	$2.3{\times}10^{-3}$	0.0520	−1.0002	7812
−1.50	217	0.97952	$1.1{\times}10^{-2}$	$3.1{\times}10^{-3}$	0.0524	−1.0005	956.5
−1.60	173	0.99421	$2.0{\times}10^{-2}$	$5.0{\times}10^{-3}$	0.0532	−1.0008	399.4
−2.00	93	1.00193	$7.1{\times}10^{-2}$	$1.5{\times}10^{-2}$	0.0559	−1.0017	162.2
−2.50	59	1.00383	$1.5{\times}10^{-1}$	$3.4{\times}10^{-2}$	0.0584	−1.0030	88.61
−3.00	44	1.00561	$2.3{\times}10^{-1}$	$6.1{\times}10^{-2}$	0.0604	−1.0052	98.29

Table 3: The fixed point solution G_{0b} of (32) for $\lambda \leq 0$ for $L = 2000$ sample points.

4.3 Varying $\lambda \leq 0$: Consistency and evidence for phase transition

Next we study the dependence of G_{0b} and G_{aa} on $\lambda \leq 0$. As before we start with $G^0_{0b} = 1$ and run the iteration until $|G^{\mathtt{i}} - G^{\mathtt{i}-1}|_\infty < 4 \times 10^{-8}$. The results are listed in table 3 for

$L = 2000$ sample points. We partly use these results in [14] to check that $G^{\mathtt{i}}$ falls into the expected region $\exp(\mathcal{K}_\lambda)$ given in (3) *although we start from* $G^{\mathtt{0}} = 1$ *which should be an exact solution for* $\Lambda^2 \to \infty$ *[14, Appendix A].* We therefore conclude that at finite Λ the difference between $G^1_{0b} = \frac{1}{1+\frac{b}{1+|\lambda|\Lambda^2}}$ and $G^0_{0b} = 1$ is enough to drive the iteration away from 1 and into another fixed point solution $G^\infty_{0b} \neq 1$. We find a monotonic convergence[5] of $\{G^{\mathtt{i}}\}$ for $\mathtt{i}$ sufficiently large. Together with the boundedness of $\{G^{\mathtt{i}}\}$ proved in [14], monotonicity (if rigorously proved) is enough for uniqueness of the fixed point soulution.

We notice that the relative asymmetry is roughly constant at a few percent and thus much smaller than for $\lambda > 0$ (see fig. 2). This is a clear signal that the sector $\lambda > 0$ is affected by the undetermined quantities C_{λ,Λ^2} and $f_{\lambda,\Lambda^2}(b)$ of (18) whereas the sector $\lambda < 0$ is completely determined.

The most striking observation is the behaviour of the finite wavefunction renormalisation $\mathcal{Y} = \mathcal{Y}_1$ which determines $\frac{dG_{0b}}{db}\big|_{b=0} = -(1+\mathcal{Y})$. As shown in fig. 5 (which also includes $\lambda > 0$), $\mathcal{Y}(\lambda)$ *undergoes a second order phase transition at* $\lambda_c \approx 0.39$ where $\mathcal{Y}'(\lambda)$ is discontinuous. To be precise, there is no discontinuity in $\mathcal{Y}'(\lambda)$ at finite cut-off $\Lambda^2 = \mathtt{co}$, only a large jump. Fig. 6 shows $\mathcal{Y}'(\lambda)$ as function of $\pi\lambda$, where $\mathcal{Y}(\pi\lambda)$ is obtained

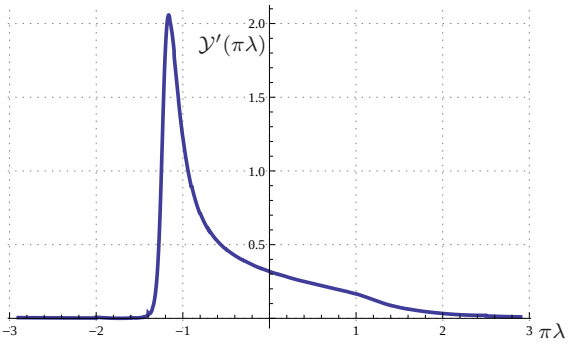

Figure 6: Plot of $\mathcal{Y}'(\lambda)$ as function of $\pi\lambda$.

by cubic interpolation of tables 2 and 3. The maximum $\mathcal{Y}'(\pi\lambda_{\max}) = 2.058$ is attained at $\pi\lambda_{\max} = -1.163$, i.e. $\lambda_{\max} = -0.370$, and the half value $\mathcal{Y}'(\pi\lambda_h) = \frac{1}{2}\mathcal{Y}'(\pi\lambda_{\max})\big|_{\lambda_c<\lambda_{\max}}$ at $\pi\lambda_h = -1.246$. Combined with results on the Stieltjes property we assign the value $\lambda_c \approx -0.39$, i.e. $\pi\lambda_c \approx -1.225$ as critical coupling constant. Another possibility would be the point $\mathcal{Y}(\lambda_0) = -1$ for which we find $\lambda_0 \approx -\frac{1.432}{\pi} \approx -0.455$. At λ_0 all higher correlation functions, in particular λ_{eff} become singular[6]. It came as surprise to us that the iteration is still convergent for $\lambda < \lambda_0$. Even more surprising is that $\mathcal{Y}(\lambda) \approx \mathcal{Y}(\lambda_0) = -1$ stays

[5]For $\lambda > 0$ there was always an alternating convergence $G^{\mathtt{i}} < G^{\mathtt{i+2}} < G^{\mathtt{i+3}} < G^{\mathtt{i+1}}$ (for $\mathtt{i}$ either even or odd.

[6]Note that λ_0 is far beyond the pole λ_B of Borel resummation of planar graphs. This pole is given as $\hat{\lambda} = -\frac{1}{12}$ in the literature, but for the normalisation $-\frac{\hat{\lambda}}{4!}\phi^4$ of the quartic interaction whereas we worked with $-\frac{\lambda}{4}\phi^4 = -\frac{6\lambda}{4!}\phi^4$. This means that the Borel pole would be at $6\lambda_B = -\frac{1}{12}$, i.e. $\lambda_B = -\frac{1}{72} = -0.013888\ldots$. We cannot identify any particular behaviour at λ_B.

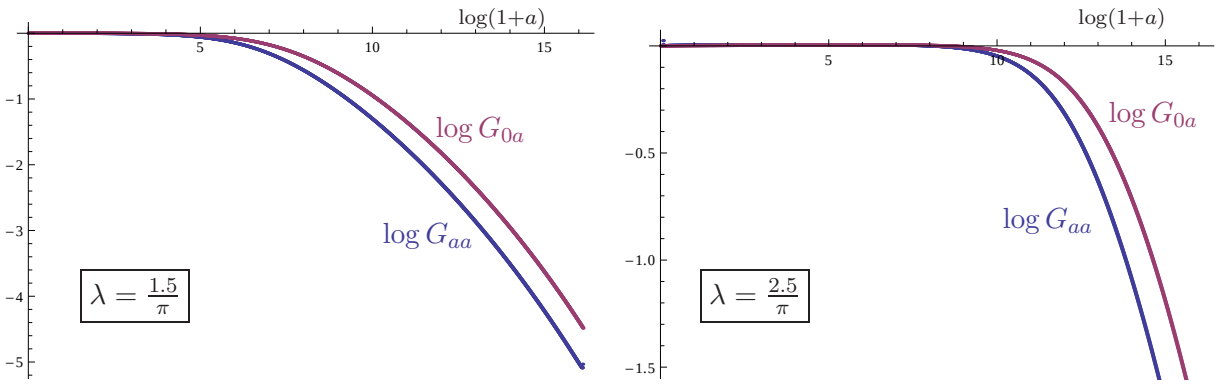

Figure 7: Plot of $\log G_{0a}$ (red) and $\log G_{aa}$ (blue) as function of $\log(1+a)$ for $\lambda < \lambda_c$.

roughly constant for $\lambda < \lambda_0$. In fact, within the reliability bound given by the relative asymmetry of 5% we can regard $\mathcal{Y}(\lambda) = -1$ for all $\lambda \leq \lambda_c$. This is also supported by fig. 7 which shows plots of both G_{0a}, G_{aa} over a for $\lambda > \lambda_c$. We notice that both G_{0a}, G_{aa} and in fact also G_{ab} all equal 1 within the reliability bound of 5% for $0 \leq a, b \leq A(\lambda)$. In other words, the exact solution $G_{0b} = 1$ of [14, Appendix A] becomes stable for $b \in [0, A(\lambda)]$. The end point $A(\lambda) = \sup\{b \ : G_{0b} = 1\}$ serves as an order parameter: We have $A(\lambda) = 0$ in the phase $\lambda_c < \lambda \leq 0$ and $A(\lambda) > 0$ for $\lambda < \lambda_c$.

For some values of λ we have computed G_{0b} at finer resolution, see table 4. We notice a considerable improvement of the asymmetry[7], whereas G_{0b}, $\mathcal{Y}$ and λ_{eff} are nearly independent of L.

4.4 The Stieltjes property of the 2-point function

Necessary for reflection positivity is that $a \mapsto G_{aa}$ is a Stieltjes function [10], which by [13] is equivalent to $L_{n,t}[G_{\bullet\bullet}] \geq 0$ for all n, t. These functions (36) are implemented in **In[12]** using an interpolation method. We have shown results for several values of $\lambda < 0$ in [16, Fig. 3]. These interpolation results allowed to exclude the Stieltjes property for $\lambda < -\frac{1.25}{\pi} \approx -0.398$. For $\lambda > 0$ we already have $L_{1,t}[G_{\bullet\bullet}] < 0$ for sufficiently large t. Hence there remained a window $\lambda \in [-0.398, 0]$ where the interpolation results were not conclusive. In this paper we investigate the remaining window by means of the formulae of Proposition 6.

It turns out that our numerical results based on the *Mathematica*^{TM} implementation in Appendix A are affected by systematic discretisation errors. These errors are unavoidable. The Stieltjes property or the (weaker but better accessible) complete monotonicity property encode a strong form of analyticity in the cut plane $\mathbb{C} \setminus]-\infty, 0]$ or the half space $\mathrm{Re}(z) > 0$, respectively. A piecewise-linear approximation cannot share such properties. But because we test the decisive properties by integral formulae, we expect that at finer resolution L and larger cut-off Λ^2 we recover more and more the true behaviour of the

[7] $G_{\Lambda^2,b}$ differs significantly from G_{b,Λ^2} so that we measure the relative asymmetry only for $a, b < \Lambda^2$.

Approximation $G^{\mathtt{i}}$ as function of λ and L, with $\sup_b \lvert G^{\mathtt{i}}_{0b} - G^{\mathtt{i}-1}_{0b}\rvert < 4{\times}10^{-8}$ `co=10^7`, `infty=10^(10)`								
$\lambda\pi$	`len`	`i`	$G^{\mathtt{i}}_{0,100}$	$G^{\mathtt{i}}_{0,\mathtt{co}}$	`AbsAsm`	`RelAsm`	$\mathcal{Y}$	$\lambda_{\mathit{eff}}\pi$
-0.80	2000	83	0.04199	$7.4{\times}10^{-6}$	$9.0{\times}10^{-6}$	0.0437	-0.3620	-0.864
-0.80	10000	3	0.04199	$7.4{\times}10^{-6}$	$5.9{\times}10^{-7}$	0.0385	-0.3620	-0.864
-0.80	40000	2	0.04199	$7.4{\times}10^{-6}$	$5.4{\times}10^{-7}$	0.0350	-0.3620	-0.864
-0.90	2000	113	0.05582	$1.5{\times}10^{-5}$	$1.5{\times}10^{-5}$	0.0454	-0.4416	-1.009
-0.90	10000	13	0.05582	$1.5{\times}10^{-5}$	$1.2{\times}10^{-6}$	0.0399	-0.4415	-1.009
-0.90	40000	5	0.05582	$1.5{\times}10^{-5}$	$1.1{\times}10^{-6}$	0.0361	-0.4415	-1.009
-1.00	2000	162	0.08016	$3.4{\times}10^{-5}$	$2.6{\times}10^{-5}$	0.0470	-0.5459	-1.196
-1.00	10000	35	0.08015	$3.4{\times}10^{-5}$	$2.9{\times}10^{-6}$	0.0411	-0.5458	-1.196
-1.00	40000	12	0.08015	$3.4{\times}10^{-5}$	$2.6{\times}10^{-6}$	0.0370	-0.5458	-1.196
-1.05	2000	200	0.10071	$5.5{\times}10^{-5}$	$3.4{\times}10^{-5}$	0.0476	-0.6132	-1.321
-1.05	10000	52	0.10069	$5.5{\times}10^{-5}$	$4.8{\times}10^{-6}$	0.0416	-0.6131	-1.321
-1.05	40000	20	0.10069	$5.5{\times}10^{-5}$	$4.3{\times}10^{-6}$	0.0374	-0.6130	-1.321
-1.10	2000	251	0.13275	$9.4{\times}10^{-5}$	$4.9{\times}10^{-5}$	0.0483	-0.6947	-1.490
-1.10	10000	78	0.13270	$9.4{\times}10^{-5}$	$8.2{\times}10^{-6}$	0.0421	-0.6945	-1.490
-1.10	40000	34	0.13270	$9.4{\times}10^{-5}$	$7.4{\times}10^{-6}$	0.0378	-0.6945	-1.490
-1.15	2000	320	0.18679	$1.7{\times}10^{-4}$	$7.7{\times}10^{-5}$	0.0489	-0.7912	-1.737
-1.15	10000	117	0.18665	$1.7{\times}10^{-4}$	$1.5{\times}10^{-5}$	0.0426	-0.7909	-1.737
-1.15	40000	56	0.18665	$1.7{\times}10^{-4}$	$1.4{\times}10^{-5}$	0.0382	-0.7909	-1.737
-1.22	2000	420	0.34038	$4.9{\times}10^{-4}$	$1.9{\times}10^{-4}$	0.0497	-0.9253	-2.279
-1.22	10000	192	0.33979	$4.9{\times}10^{-4}$	$4.4{\times}10^{-5}$	0.0432	-0.9248	-2.287
-1.22	40000	103	0.33976	$4.9{\times}10^{-4}$	$3.9{\times}10^{-5}$	0.0387	-0.9248	-2.288

Table 4: The fixed point solution G_{0b} of (32) for $\lambda \leq 0$ for various resolutions `len`$= L$. Finer resolutions provide a significant decrease of asymmetry. The iteration for `len=2000` starts with $G^0_{0b} = 1$, whereas for `len=10000` and `len=40000` we start with G^0_{0b} given by an interpolation of the previous $G^{\mathtt{i}}_{0b}$ at `len=2000` and `len=10000`, respectively. The values for `len=40000` had a total computation time of 4 months!

solution. Our numerical results confirm this expectation and thus provide strong support, albeit no proof, of the following

Conjecture 7 *The diagonal matrix 2-point function G_{aa} of the $\lambda\phi^4_4$-model on noncommutative Moyal space in the limit of infinite noncommutativity is a Stieltjes function for $\lambda_c < \lambda \leq 0$.*

We first provide some checks for the correctness of Proposition 6 and its implementation. We show in fig. 8 for the function $C^n_0(a)$ defined in (51) a comparison between the numerical differentiation of $\cot \tau_0(a)$ and the integral formula. In fig. 9 we compare for the function $\frac{(-a)^n}{n!}\frac{d^n}{da^n}(\mathrm{sign}(\lambda)\mathcal{H}^{\tilde{\Lambda}}_a[\tau_0(\bullet)])$ the numerical differentiation with the integral formula (which is (54) without the $L^{(n,\ell)}(a,b)$-term taken at $\ell = 0$ and $b = 0$, and with

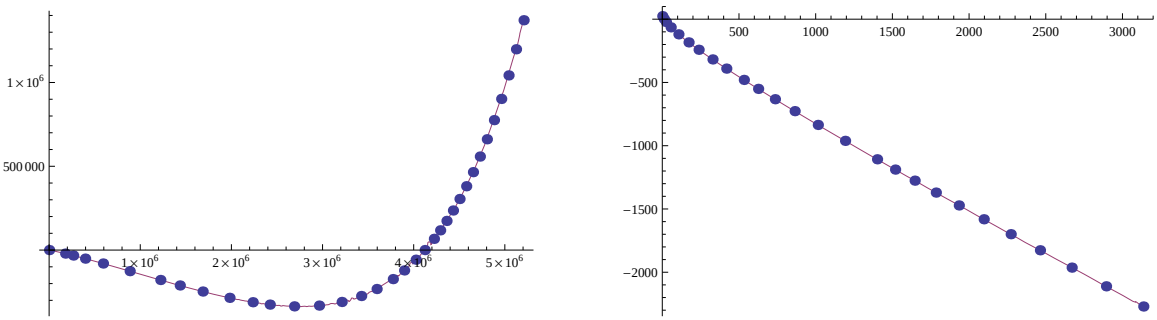

Figure 8: Comparison of interpolation (solid line) and integral formulae (dots) for $C_0^2(a)$ (left) and $C_0^4(a)$ (right) at $\lambda\pi = -1.25$. The integral formulae are based on $\Lambda^2 = 10^7$ and $L = 2000$ sample points.

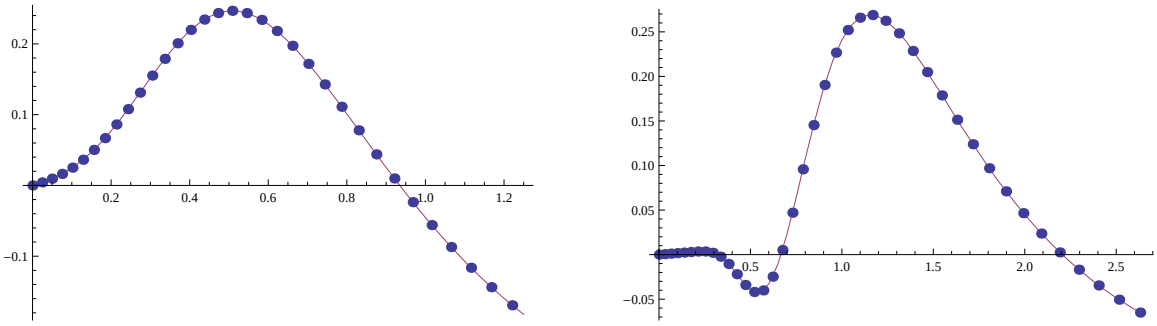

Figure 9: Comparison of interpolation (solid line) and integral formulae (dots) for $\frac{(-a)^2}{2!}\frac{d^2}{da^2}(\mathrm{sign}(\lambda)\mathcal{H}_a^{\tilde{\Lambda}}[\tau_0(\bullet)])$ (left) and $\frac{(-a)^5}{5!}\frac{d^5}{da^5}(\mathrm{sign}(\lambda)\mathcal{H}_a^{\tilde{\Lambda}}[\tau_0(\bullet)])$ (right) at $\lambda\pi = -1.10$, $\Lambda^2 = 10^7$ and $\tilde{\Lambda}^2 = (10^7+1)^{\frac{3}{5}} - 1$. The integral formulae are based on $L = 2000$ sample points.

insertion of (52)). For small a this function should be independent of the cut-off $\tilde{\Lambda}$. We confirm in table 5 that, as long as $\tilde{\Lambda}^2 \gg a$ and up to boundary artifacts for $\tilde{\Lambda}^2 = \Lambda^2$, the function $A^{(n,\ell)}$ is indeed independent of $\tilde{\Lambda}^2$. We use this independence in order to take a comparably low value $K = 1200$, corresponding to $1 + \tilde{\Lambda}^2 = (1 + \tilde{\Lambda}^2)^{\frac{3}{5}}$, for our simulation in order to save computing time.

The strongest support for Conjecture 7 comes from the observation that the critical indices

- $n^{\mathcal{L}0} = \min\{n \ : \ (-1)^n (\log G_{0b})^{(n)}\big|_{b=0} < 0\}$,
- $n^{\mathcal{L}} = \min\{n \ : \ (-1)^n (\log G_{0b})^{(n)} < 0 \text{ for some } b\}$ where logarithmically complete monotonicity of G_{0b} fails,
- $n^{\mathcal{C}} = \min\{n \ : \ (-1)^n G_{0b}^{(n)} < 0 \text{ for some } b\}$ where complete monotonicity of G_{0b} fails,
- $n_0^{\mathcal{S}} = \min\{n \ : \ L_{n,t}(G_{0\bullet}) < 0 \text{ for some } t\}$ where the Stieltjes property of G_{0b} fails,
- $n^{\mathcal{S}} = \min\{n \ : \ L_{n,t}(G_{\bullet\bullet}) < 0 \text{ for some } t\}$ where the Stieltjes property of G_{aa} fails,

K	(n,ℓ)=(6, 1)	(n,ℓ)=(5, 0)	(n,ℓ)=(0, 5)	(n,ℓ)=(1, 0)	(n,ℓ)=(0, 1)
50	2.40622	−6.21325	0.0000129836	−0.556715	−0.0065814
80	0.00182617	−0.00479778	0.0000162935	−0.0837978	−0.0548360
100	0.00145747	−0.00021191	0.0000170968	−0.0149419	−0.0714913
150	0.00143641	0.000222779	0.0000171231	0.0426437	−0.0931625
200	0.00143644	0.000229322	0.0000171114	0.0592362	−0.102702
400	0.00143644	0.000229763	0.0000171104	0.0724140	−0.113218
800	0.00143643	0.000229765	0.0000171104	0.0743314	−0.115140
1200	0.00143643	0.000229765	0.0000171104	0.0744010	−0.115211
1800	0.00143643	0.000229765	0.0000171104	0.0744037	−0.115214
1900	0.00143643	0.000229764	0.0000171104	0.0744037	−0.115214
1990	0.00143643	0.000229636	0.0000171104	0.0744037	−0.115214
2000	0.00143643	0.00474417	0.0000171104	0.0744037	−0.115214

Table 5: $A^{(n,\ell)}(x_{40}, x_{20})$ for $\lambda\pi = -1.10$ as function of the secondary cutoff $\tilde{\Lambda}^2 = x_K$. The primary cut-off is $x_{L+1} = 10^7$ with $L = 2000$.

satisfy for all tested values of L and λ the following relations:

$$n^{\mathcal{L}0} = n^{\mathcal{L}} \ , \quad n^{\mathcal{C}} \gtrapprox n^{\mathcal{L}} \ , \quad n_0^{\mathcal{S}} \geq n^{\mathcal{C}} + 1 \ . \tag{56}$$

Our results are given (together with $n^{\mathcal{S}}$ discussed below) in table 6. The computation of $n^{\mathcal{L}0}$ is fast and therefore to perform to large values. We can then look at $(-1)^n(\log G_{0b})^n$ for $n \in \{n^{\mathcal{L}0}, n^{\mathcal{L}0} - 1\}$ and notice that the first wrong sign always arises for $b = 0$. The computation of $n^{\mathcal{C}}$ involves via the Bell polynomials $Y_{n,k}$ a sum over all partitions of n. For $n \gtrapprox 80$ this cannot be done anymore in reasonable time. For the same reason we can only test $n_0^{\mathcal{S}} \lessapprox 40$. The relation $n^{\mathcal{C}} \geq n^{\mathcal{L}}$ is clear by definition. But $n_0^{\mathcal{S}}$ and $n^{\mathcal{C}}$ are, a priori, uncorrelated because a typical completely monotonic function has no reason to be Stieltjes. The observed relation $n_0^{\mathcal{S}} \geq n^{\mathcal{C}} + 1$ is therefore extremely strong support for the claim that a completely monotonic solution of (32) is automatically Stieltjes for $\lambda_c < \lambda \leq 0$. Together with the observed dependence of $1 + \mathcal{Y}_n = \frac{(-1)^n}{(n-1)!}(\log G_{0b})^{(n)}\big|_{b=0}$ on n, shown for selected values of λ and L in fig. 10, we have overwhelming support for the assertion that *the exact solution G_{0b} of (32) is a Stieltjes function for $\lambda_c < \lambda \leq 0$*. Near the critical coupling constant λ_c the improvement at higher resolution L slows down. In agreement with previous considerations on the discontinuity of $\frac{d\mathcal{Y}}{d\lambda}$ we confirm that $\lambda = -\frac{1.22}{\pi} \approx -0.388$ is already very close to λ_c, which we would define as the critical value where a finite $n^{\mathcal{L}}(\infty)$ remains. The curves in fig. 10 suggest that for $0 \leq b \leq 1$ one has a power series representation

$$G_{0b} = \exp\Big(\sum_{n=1}^{\infty} \frac{(-1)^n}{n} c_n b^n\Big) \ , \ (c_n)_n \text{ positive monotonously decreasing null sequence} \ . \tag{57}$$

Our main interest is the diagonal 2-point function G_{aa}. Due to much larger numerical errors we can only give qualitative results. For instance, the value $n_0^{\mathcal{S}}$ at $\lambda = -\frac{1}{\pi}$ and

$\lambda\pi$	L	$n^{\mathcal{L}0}$	$n^{\mathcal{L}}$	$n^{\mathcal{C}}$	$n_0^{\mathcal{S}}$	$n^{\mathcal{S}}$
-0.80	2000	109	109			
-0.80	10000	179	179			
-0.80	40000	266	266			
-0.90	2000	58	58			
-0.90	10000	95	95			
-0.90	40000	137	137			
-1.00	2000	31	31	35	37	
-1.00	10000	49	49	55		
-1.00	40000	69	69	75		
-1.05	2000	22	22	25	26	≥ 11
-1.05	10000	34	34	38	39	
-1.05	40000	47	47	51		
-1.10	2000	15	15	17	18	≥ 11
-1.10	10000	23	23	25	26	
-1.10	40000	30	30	33	34	
-1.15	2000	9	9	10	11	8
-1.15	10000	14	14	15	16	> 10
-1.15	40000	18	18	20	21	
-1.20	2000	6	6	6	7	6
-1.22	2000	5	5	5	6	5
-1.22	10000	6	6	7	8	6
-1.22	40000	7	7	9	10	

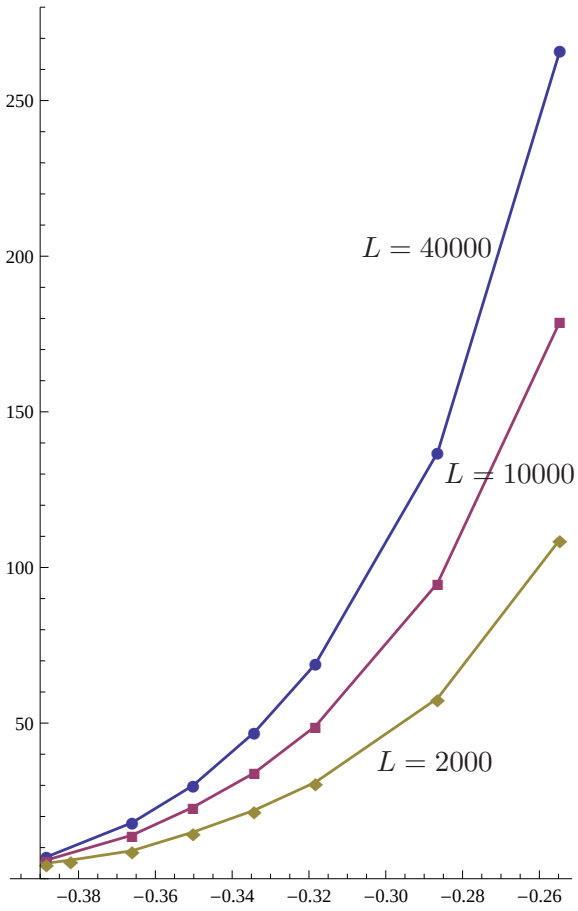

Table 6: The critical indices where Stieltjes and complete monotonicity properties fail, as function of λ and of the number L of sample points. Because of discretisation errors we define $n^{\mathcal{S}}$ in a coarse manner in (58), and due to noise we can only give lower bounds in some cases. The figure shows $n^{\mathcal{L}}$ as function of L and λ.

$L = 2000$ results from $L_{37,x_2}(G_{0\bullet}) = -1.36 \times 10^{-57}$. If we apply such strict criteria to G_{aa} then G_{aa} fails to be logarithmically completely monotonic already at very low n. As we describe below, there are clear hints that these wrong signs are due to noise and systematic discretisation errors. The values of $n^{\mathcal{S}}$ in Table 6 do not reflect its strict definition but show the critical index where the curve $L_{n,t}(G_{\bullet\bullet})$ becomes "visibly" negative for some t. Fig. 11 shows these curves for typical values of λ and n. We notice that for $0 \leq t < t_0(\lambda)$, the sequence $L_{n,t}[G_{\bullet\bullet}]$ converges to zero (which reflects a mass gap). Any small noise of the zero function produces values < 0. Therefore we discard the interval $[0, t_0]$ from our definition of $n^{\mathcal{S}}$,

$$n^{\mathcal{S}} := \min\{n \,:\, L_{n,t}[G_{\bullet\bullet}] < 0 \text{ for some } t \geq t_0(n) := \inf\{s \,:\, L_{s,n}[G_{\bullet\bullet}] > 3 \cdot 10^{-4}\}\} \,. \quad (58)$$

In this way we require a certain amount of oscillation for a violation of the Stieltjes property. For $n \geq 12$ and $L = 2000$ the noise is so large that we even violate the coarse

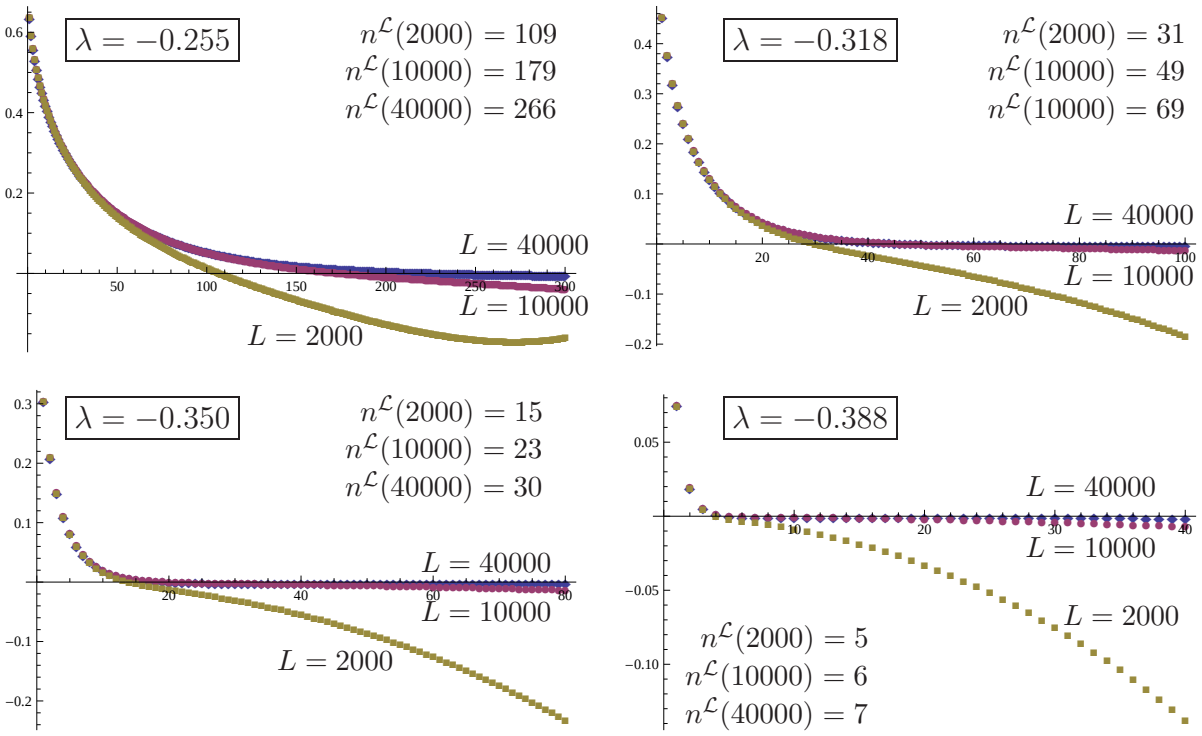

Figure 10: Plots of $\frac{(-1)^n}{(n-1)!}(\log G_{0b})^{(n)}\big|_{b=0}$ as function of n for various resolutions L. The boundary 2-point function G_{0b} is logarithmically completely monotonic if these curves are positive for all n. The discretisations fail this property at a critical index $n^{\mathcal{L}0}(L)$.

condition. For $-1.22 \leq \lambda\pi \leq -1.15$ and $L = 2000$ the plots of $L_{n,t}(G_{\bullet\bullet})$ become coarsely negative before the noise sets in. We are convinced that also these visible oscillations are discretisation artifacts. In fig. 12 we show that for small $|\lambda|$ there is excellent agreement between the interpolation formula and the integral formula of $L_{n,t}[G_{\bullet\bullet}]$. For larger $|\lambda|$, as shown in fig. 13, we notice a severe discrepancy which by far exceeds our typical reliability region of 5%. We think that for smaller $|\lambda|$ this discrepancy is still present in $L_{n,a}[G_{\bullet\bullet}]$ but for larger n, leading to the oscillations noticed in fig. 11. The reason is that both $\mathrm{sign}(\lambda)\mathcal{H}_a^{\tilde{\Lambda}}[\tau_b(\bullet)]$ and $\log\frac{\sin\tau_b(a)}{|\lambda|\pi a}$ have large derivatives but of opposite sign which almost compensate each other. Errors of 5% in each of $\mathrm{sign}(\lambda)\mathcal{H}_a^{\tilde{\Lambda}}[\tau_b(\bullet)]$ and $\log\frac{\sin\tau_b(a)}{|\lambda|\pi a}$ can thus make their sum to $(\log G_{aa})^{(n)}$ unreliable.

At finer resolution L the discretisation error should improve. This is clearly visible in fig. 14 which compares $L_{n,t}[G_{\bullet\bullet}]$ for iterations with the same values $\lambda = -\frac{1.22}{\pi}$, $\Lambda^2 = 10^7$ and $\tilde{\Lambda}^2 = (\Lambda^2+1)^{\frac{3}{5}} - 1 \approx 15848$; but with $L = 2000$ versus $L = 10000$ sample points. Whereas the critical index $n^{\mathcal{S}}$ (coarsely defined by (58)) where the Stieltjes property is lost increases only from $n^c = 5$ at $L = 2000$ to $n^c = 6$ at $L = 10000$, the curves differ dramatically. Fig. 15 is the analogue of the first row in fig. 11 for the resolution $L = 10000$. For $\lambda\pi = -1.15$ we have up to $n = 10$ no hint of a visible oscillation, whereas for $L = 2000$ we had a failure already at $n^{\mathcal{S}} = 8$. All this is overwhelming support for the conjecture

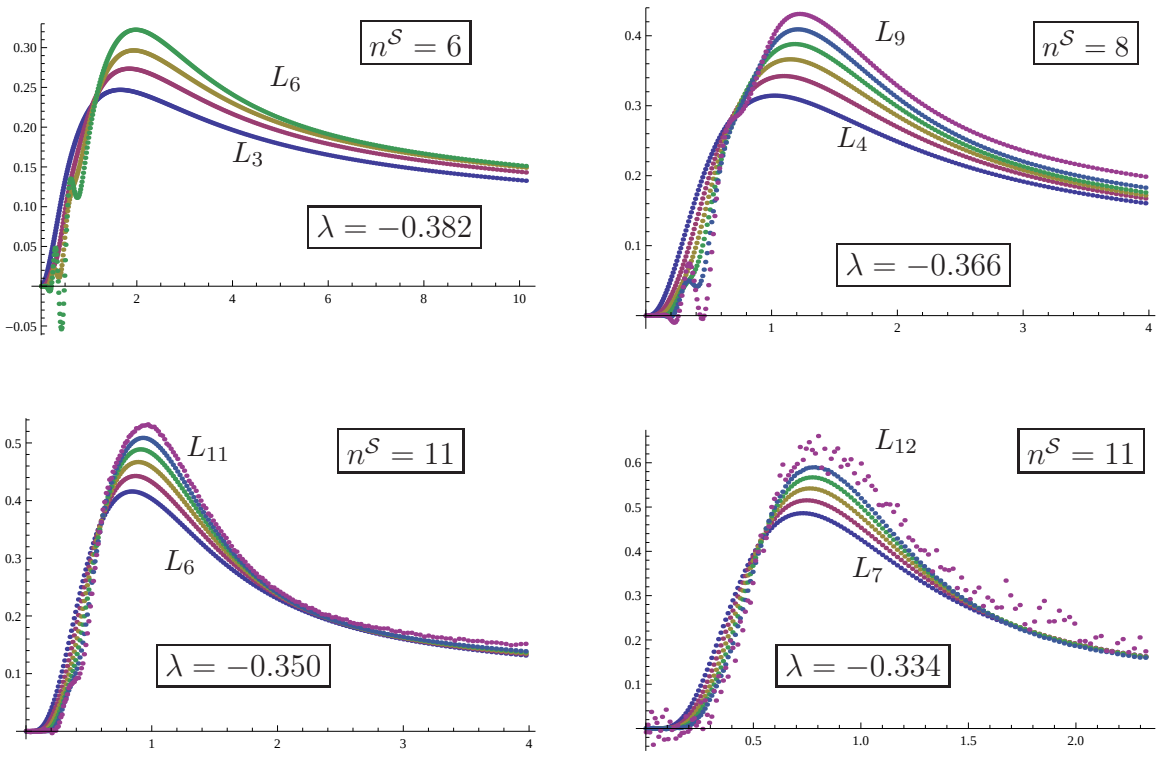

Figure 11: Widder's operations $L_{n,t}[G_{\bullet\bullet}]$ at $\lambda\pi \in \{-1.20,\ -1.15,\ -1.10,\ -1.05\}$ and $L = 2000$ sample points. In order to define a Stieltjes function, $L_{n,t}$ has to be non-negative for all n and t. For $n \geq 12$ there is too much noise to be conclusive. At $\lambda\pi \in \{-1.20,\ -1.15\}$ the curves turn negative, but also these oscillations are possibly discretisation artifacts.

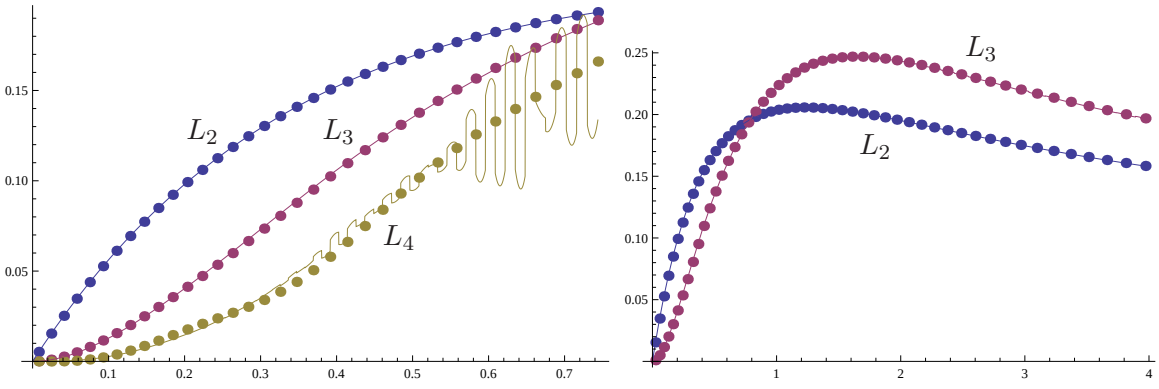

Figure 12: Comparison of interpolation (solid line) and integral formulae (dots) for $L_{n,a}[G_{\bullet\bullet}]$ at $\lambda\pi = -1.20$. The integral formulae are based on $\Lambda^2 = 10^7$ and $L = 2000$ sample points.

that for the exact solution of the master equation (i.e. $L \to \infty$) the critical index $n^{\mathcal{S}}$ diverges for $\lambda_c < \lambda \leq 0$.

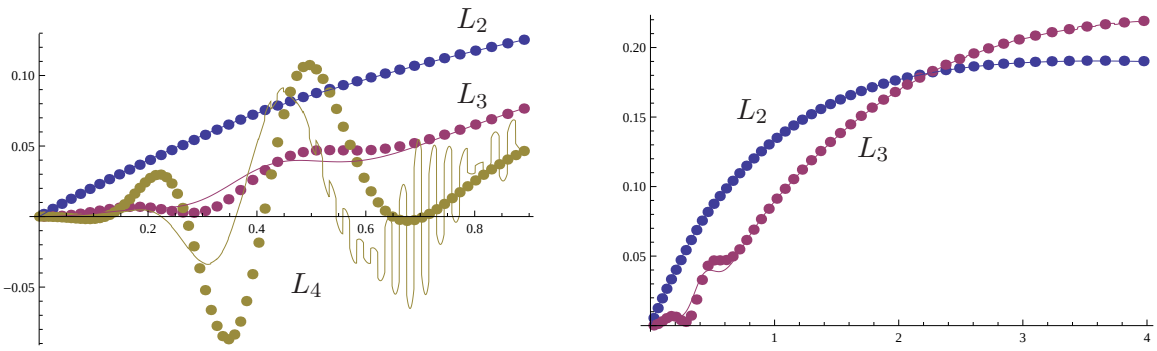

Figure 13: Comparison of interpolation (solid line) and integral formulae (dots) for $L_{n,a}[G_{\bullet\bullet}]$ at $\lambda\pi = -1.25$. The integral formulae are based on $\Lambda^2 = 10^7$ and $L = 2000$ sample points. There is a clear discrepancy already in $L_{3,a}$ in the interval $a \in [0.15, 0.7]$ which becomes dramatic in L_4. For larger a the agreement improves, subject to noise in the interpolation.

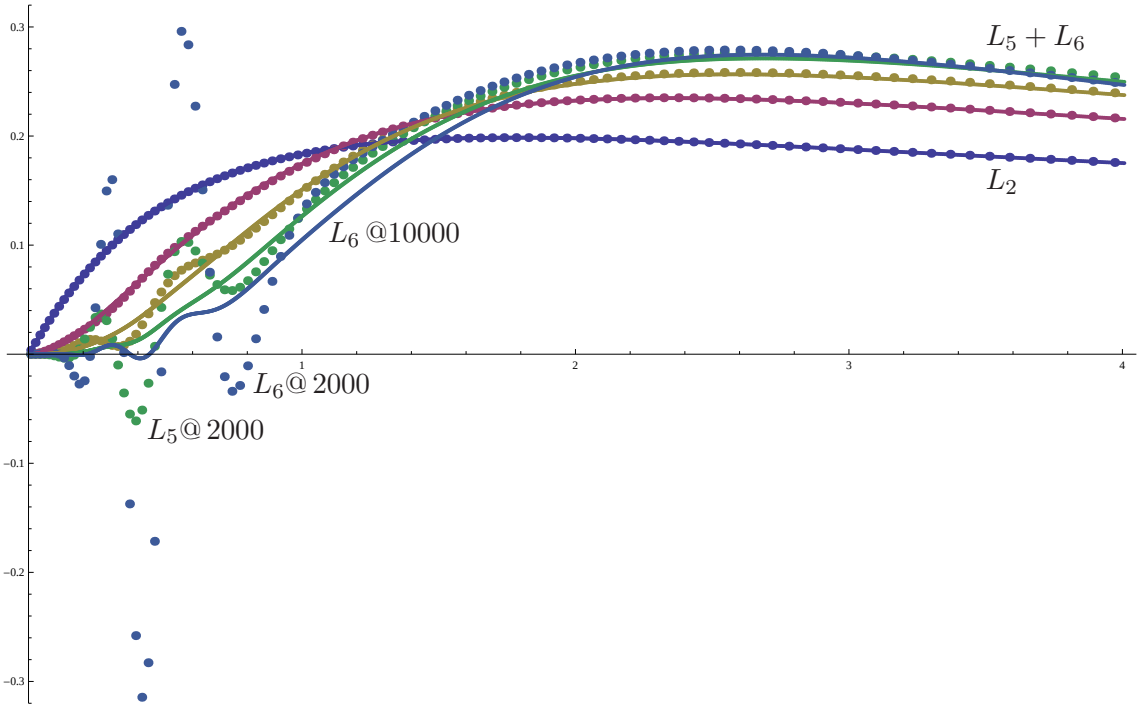

Figure 14: $L_{n,t}[G_{\bullet\bullet}]$ for $\lambda = -\frac{1.22}{\pi}$, $\Lambda^2 = 10^7$ and $\tilde{\Lambda}^2 = 15848$, but with $L = 2000$ (squares) versus $L = 10000$ sample points (solid curves).

5 Conclusions

In summary, we are convinced that Conjecture 7 is true. A proof is impossible by numerical methods, but the simulations gave us a clear strategy how to proceed. One should first prove that the fixed point equation (32) has for $\lambda < 0$ a unique *stable* solution G_{0b}

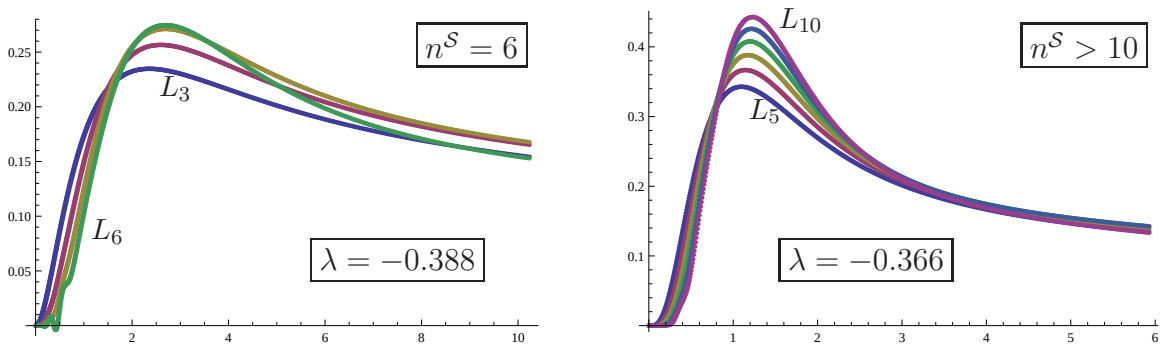

Figure 15: Widder's operations $L_{n,t}[G_{\bullet\bullet}]$ at $\lambda\pi \in \{-1.22,\ -1.15\}$ and $L = 10000$ sample points. These plots need much computation time so that $L_{n,t}$ is not yet available for $n > 10$.

inside $\exp(\mathcal{K}_\lambda)$, and that this solution is Stieltjes. Our numerical results leave no doubt that this is the case. The further steps, symmetry $G_{ab} = G_{ba}$ and Stieltjes property of G_{aa} should then make use of the Stieltjes representation of G_{0b}.

Suppose all this succeeds and the Schwinger 2-point function $\mathcal{S}_c(\mu x_1, \mu x_2)$ defined in (34) is reflection positive. Then one has to pass to the higher functions $G_{a_1 \ldots a_1 | \ldots | a_B \ldots a_B}$. These are given by algebraic recursion formulae [6] if one of the cycles $a_i \ldots a_i$ consists of ≥ 4 indices, but solve their own linear singular integral equations[8] if all cycles have length 2. A representation of G_{0b} as a Stieltjes transform will help to control positivity of these solutions, but there is no guarantee that this is enough. It might be necessary to have an explicit formula for G_{0b} in terms of known functions. We have looked for such a formula in various directions; so far without success.

Suppose that all this leads to a proof of reflection positivity for the family (34) of Schwinger functions. The Osterwalder-Schrader theorem [12] then reconstructs Wightman functions of a relativistic quantum field theory [19]. The final problem is then to decide between triviality or non-triviality of the model. The Schwinger functions (34) do not permit momentum transfer, which in 4 dimensions is usually a sign of triviality. However, the model has two features which might circumvent the triviality theorems: Absence of clustering and absence of a second gap $]m^2, 4m^2[$ in the mass spectrum (deduced from an extrapolation of $L_{n,t}[G_{\bullet\bullet}]$ to $n = \infty$ in figs. 11 and 15). On the other hand, absence of momentum transfer is a generic feature of any integrable model [20, 21]. One cannot expect the richness of two-dimensional integrable models: The Schwinger functions (34) do not depend on $\langle p_i, p_j \rangle$ for $i \neq j$ so that the S-matrix cannot depend on rapidities. At best the model decomposes into different vacuum sectors (no clustering!), and in each sector the S-matrix is a sector-dependent pure phase $S = e^{\mathrm{i}\alpha}$. But even such a simple S-matrix is outside the scope of any other four-dimensional quantum field theory we know

[8] The (2+2)-point function $G_{ab|cd}$ involves an auxiliary function that solves the linear singular integral equation [6, eq. (A.20a)]. Contrary to the statement in [6], this equation is not of Carleman type, but the solution techniques of [7, 8] allow to regularise this equation to an integral equation of Fredholm type which always has a unique solution for $|\lambda|$ small enough.

of. This provides enough motivation to proceed.

Acknowledgements

We would like to thank the Erwin-Schrödinger-Institute for Mathematical Physics in Vienna and the Collaborative Research Centre "Groups, Geometry and Actions" (SFB 878) in Münster for financing several mutual visits.

A Implementation in Mathematica^{TM}

A.1 Main definitions

We view G_{0b} as linear interpolation between an increasing sequence of sample points x_k for $k = 1, \dots L+1$, with $x_1 = 0$ and $x_{L+1} = \Lambda^2$. We let $G_{0x_k} =: G(k) =$ `lis[[k]]`. This is a Lipschitz-continuous function so that the Hilbert transform exists pointwise [22]. For $s \in [x_k, x_{k+1}]$ we have $G_{0s} := \frac{x_{k+1}-s}{x_{k+1}-x_k} G(k) + \frac{s-x_k}{x_{k+1}-x_k} G(k+1)$. We are only interested in the Hilbert transform at sample points x_n:

$$
\begin{aligned}
&\pi \mathcal{H}^{\Lambda}_{x_n}[G_{0\bullet}] \\
&= \lim_{\epsilon\to 0} \sum_{k=1}^{L} \int_{x_k+\epsilon}^{x_{k+1}-\epsilon} \frac{ds}{s-x_n} \Big(\frac{x_{k+1}-s}{x_{k+1}-x_k} G(k) + \frac{s-x_k}{x_{k+1}-x_k} G(k+1) \Big) \\
&= G(L+1) - G(1) + \lim_{\epsilon\to 0} \sum_{k=1}^{L} \int_{x_k+\epsilon}^{x_{k+1}-\epsilon} \frac{ds}{s-x_n} \Big(\frac{x_{k+1}-x_n}{x_{k+1}-x_k} G(k) + \frac{x_n-x_k}{x_{k+1}-x_k} G(k+1) \Big) \\
&= \Big(\sum_{k=1}^{n-2} + \sum_{k=n+1}^{L} \Big) \frac{(x_n-x_k)G(k+1) - (x_n-x_{k+1})G(k)}{x_{k+1}-x_k} \log\Big(\frac{x_n-x_{k+1}}{x_n-x_k} \Big) \\
&+ G(L+1) - G(1) + \begin{cases} G(1) \log \frac{x_2-x_1}{\epsilon} & \text{for } n=1 \\ G(n) \log \frac{x_{n+1}-x_n}{x_n-x_{n-1}} & \text{for } n \neq 1, L+1 \\ -G(L+1) \log \frac{x_{L+1}-x_L}{\epsilon} & \text{for } n = L+1 \end{cases}
\end{aligned}
\tag{A.1}
$$

We assume the sample points $\{x_k\}$ given as list `xi` of length $L+1 =$`len+1` with `xi[[1]]=0` and `xi[[len+1]]=co`$= \Lambda^2$. According to (A.1) we implement the finite Hilbert transform of a function given as list `lis` of length $\geq$`lng+1` as

```
In[1] Hilbert[lis_, xi_, n_, lng_] := (1/Pi)*( lis[[lng+1]]-lis[[1]] +
        Sum[If[Or[n==k, n-1==k], 0,
          ((xi[[n]] - xi[[k]])*lis[[k+1]]
              - (xi[[n]]-xi[[k+1]])*lis[[k]])/(xi[[k+1]]-xi[[k]])*
          Log[(xi[[n]]-xi[[k+1]])/(xi[[n]]-xi[[k]])]], {k, 1, lng}] +
        If[n==1, lis[[1]]*infty, If[n==lng+1, -lis[[lng+1]]*infty,
            lis[[n]] Log[(xi[[n+1]]-xi[[n]])/(xi[[n]]-xi[[n-1]])]]])
```

We set both $\frac{x_2-x_1}{\epsilon}$ and $\frac{x_{L+1}-x_L}{\epsilon}$ to the number `infty`. We usually have `lng=len` $= L$; only later for the Stieltjes property we need another cut-off. The next step is to implement the angle function (14). We assume that $\{G_{0x_k}\}$ and $\{\mathcal{H}^\Lambda_{x_k}[G_{0\bullet}]\}$ are given as lists `lis` and `hilb` of length `len+1`. The coupling constant is `la`$= \lambda$. Then $\tau_{x_b}(x_a)$ given by (14) is implemented as

```
In[2] CorrAT[x_] := If[x >= 0 , x, Pi+x];
      Tau[lis_, hilb_, xi_, a_, b_] := CorrAT[ArcTan[
          (Abs[la] Pi xi[[a]])/(xi[[b]] +
              (1 + la Pi xi[[a]] hilb[[a]])/lis[[a]] )]]]
```

The function `CorrAT` moves the branch of the arctan into the interval $[0, \pi]$.

Always for $\lambda < 0$ and under the assumption $f_{\lambda,\Lambda^2}(b) = 0$ also for $\lambda > 0$, the equation (19) is a fixed point equation $G = \tilde{T}G$ for the boundary 2-point function G_{0b}. Its solution gives the full 2-point function G_{ab} via (18), always for $\lambda < 0$ and for $\lambda > 0$ under the additional assumption $C_{\lambda,\lambda^2} = f_{\lambda,\lambda^2}(b) = 0$. We thus implement the operator $(\tilde{T}[\ ])_{0x_b}$ and the full 2-point function $G_{x_a x_b}$ as `Gout` and `Gfull`, respectively:

```
In[3] Gout[lis_, hilb_, xi_, b_] := (1/(1 + xi[[b]]))*Exp[-Sign[la]*
        Hilbert[Table[Tau[lis, hilb, xi, k, 1] -
                  Tau[lis, hilb, xi, k, b], {k, 1, len+1}], xi, 1, len]
```

```
In[4] Gfull[lis_, hilb_, xi_, a_, b_] := Exp[-Sign[la]*
        (Hilbert[Table[Tau[lis, hilb, xi, n, 1],{n, 1, len+1}],
                  xi, 1, len] -
         Hilbert[Table[Tau[lis, hilb, xi, n, b],{n, 1, len+1}],
                  xi, a, len])]*
           If[a>1, Sin[Tau[lis, hilb, xi, a, b]]/(Abs[la] Pi xi[[a]]),
                   1/(1+xi[[b]])] //Quiet
```

In principle we could spell out the Hilbert transform in (19) as an integral to obtain the master equation (32). Depending on the numerical implementation of the integration there is then the danger to violate the identity `Gfull[lis, hilb, xi, 1, b]= Gout[lis, hilb, xi, b]`. We therefore prefer (19) to (32). The result of $G_{x_a x_b}$ for x_a close to Λ^2 can become smaller than the minimal positive machine number so that we turn off the corresponding error message via `Quiet`.

We also need a few functions to control the convergence and the quality of our discrete approximation. We define supremum norm, Lipschitz seminorm, the absolute asymmetry $\sup_{a,b} |G_{x_a x_b} - G_{x_b x_a}|$ and the relative asymmetry $\sup_{a,b} \frac{|G_{x_a x_b} - G_{x_b x_a}|}{G_{x_a x_b} + G_{x_b x_a}}$:

```
In[5] SupNorm[lis1_, lis2_] :=
          Max[Table[Abs[lis1[[k]] - lis2[[k]]], {k, 1, len+1}]];
      LipNorm[lis1_, lis2_, xi_] :=
          Max[Table[Max[Table[ Abs[((lis1[[n]] - lis2[[n]]) -
                   (lis1[[k]] - lis2[[k]]))/ (xi[[n]] - xi[[k]])],
            {k, n+1, len+1}]], {n, 1, len}]];
```

```
AbsAsm[lis_, hilb_, xi_, sx_, dx_, fx_, sy_, dy_, fy_] :=
   Max[Table[Max[Table[
      Abs[Gfull[lis, hilb, xi, sx + n dx, sy + k dy] -
           Gfull[lis, hilb, xi, sy + k dy, sx + n dx]],
      {n, 0, Floor[Min[len+1-sx, fx-sx]/dx]}]],
      {k, 0, Floor[Min[len+1-sy, fy-sy]/dy]}]];
RelAsm[lis_, hilb_, xi_, sx_, dx_, fx_, sy_, dy_, fy_] :=
   Max[Table[Max[Table[ Abs[ 1-2/(1+
      Gfull[lis, hilb, xi, sx + n dx, sy + k dy]/
           Gfull[lis, hilb, xi, sy + k dy, sx + n dx])],
      {n, 0, Floor[Min[len+1-sx, fx-sx]/dx]}]],
      {k, 0, Floor[Min[len+1-sy, fy-sy]/dy]}]];
```

In order to have tolerable computing time the asymmetries need to be evaluated for a subset $\{a_k = a_0 + k\delta_1,\ b_n = b_0 + n\delta_2\}$ of indices. We search the region of maximal asymmetry by hand.

The 4-point function at vanishing arguments defines the effective coupling constant $G_{0000} = -\lambda_{\mathit{eff}}$ which according to [6] is given by

$$\lambda_{\mathit{eff}} = \frac{\lambda}{1+\mathcal{Y}_1} + \frac{\lambda^2\pi}{(1+\mathcal{Y}_1)^2}\mathcal{H}_0^\Lambda\Big[\frac{1-G_{0\bullet}}{G_{0\bullet}}\Big(\frac{\sin\tau_0(\bullet)}{|\lambda|\pi\bullet}\Big)^2\Big]\,, \tag{A.2}$$

where $\mathcal{Y}_\ell$ is defined in (47). We implement these functions as

```
In[6] calY[ell_, lis_, hilb_, xi_] := Sign[la]*Hilbert[ Table[
         Sin[ell Tau[lis, hilb, xi, n, 1]]*(If[n==1, 1,
            Sin[Tau[lis, hilb, xi, n, 1]]/(Abs[la] Pi xi[[n]])])^ell,
      {n, 1, len+1} ], xi, 1, len];
   laeff[lis_, hilb_, xi_] := la/(1 + calY[1, lis, hilb, xi]) +
      la^2 Pi/(1 + calY[1, lis, hilb, xi])^2*
          Hilbert[ Table[((1 - lis[[n]])/lis[[n]])*
               If[Or[n==1, la==0], 1,
                  Sin[Tau[lis, hilb, xi, n, 1]]^2/(la Pi xi[[n]])^2],
                {n, 1, len+1}], xi, 1, len];
```

A.2 Iteration

From a numerical simulation in an early version arXiv:1205.0465v1 of [6] we expect that $G_{b0} \approx \frac{1}{(1+b)^\eta}$ shows a power-law behaviour. This suggests to choose the sample points x_k according to a geometric progression:

```
In[7] co = 100; len = 1000; la = 1/Pi; infty = N[10^8];
      xs = Table[N[(1+co)^((n-1)/len) - 1], {n, 1, len+1}];
```

Coupling constant $\lambda =$ `la`, cut-off `co`$= \Lambda^2$ and the number `len`$= L$ of sample points will be varied; but the list of sample points will always be a geometric progression `xs`. We

have also tried equidistant samples and finer resolutions near co$=\Lambda^2$ to better deal with the singularity of the finite Hilbert transform at the boundary Λ^2; all had worse quality parameters than the geometric progression.

For definiteness of the result we start with the constant function $G^0_{0b}=1$ (which would be an exact solution for la<0 and co=∞, see [14, Appendix A]) and approximate $G_{0b}\mapsto (TG)_{0b}$ by the numerical implementation lis[[.]]↦Gout[lis,hilb,xs, .] below in **In**[**8**]:

In[**8**]
```
gs[0] = Table[1., {n, 1, len+1}];
hs[0] = Table[Hilbert[gs[0], xs, n, len], {n, 1, len+1}];
For[i=1, i<=imax, i++,
   gs[i] = Table[Gout[gs[i-1], hs[i-1], xs, b], {b, 1, len+1}];
   hs[i] = Table[Hilbert[gs[i], xs, n, len], {n, 1, len+1}];
   Print[i, " " ,
    Interpolation[Table[xs[[k]], gs[i][[k]], {k, 1, len+1}]][100],
      " " , gs[i][[-1]], " ",
      SupNorm[gs[i], gs[i-1]], " ", LipNorm[gs[i], gs[i-1],xs]];
  If[i>=20, Break[]]; ];
gfull[i]=Table[Gfull[gs[i], hs[i], xs, k, k], {k, 1, len+1}];
```

We set imax to a sufficiently large number but actually stop here at i=20. During the iteration we print out several parameters to control the quality. We notice that both supremum norm and Lipschitz seminorm improve (for $\lambda=\frac{1}{\pi}$) by a factor >3 in the step from i to i+1. This is strong support for norm convergence of the iteration. We also list the approximation of G_{0b} for $b=100$ (kept fixed when varying Λ^2) and $b=\Lambda^2$. The first value is to check the pointwise convergence of G_{0b} as $\Lambda\to\infty$. The second value affects the absolute asymmetry if Λ is chosen too small. The asymmetry is tested with the function AbsAsm for various ranges of parameters. We plot the functions G_{0b} and G_{aa} in double logarithmic coordinates:

In[**9**]
```
ListPlot[
   {Table[Log[1+xs[[k]]], Log[gfull[20][[k]]]}, {k, 1, len-40}],
     Table[{Log[1+xs[[k]]], Log[gs[20][[k]]], {k, 1, len}]},
      AxesOrigin -> {0, 0}, PlotStyle->PointSize[Tiny]]
```

These functions are decreasing and approximately linear (see fig. 1). The diagonal function G_{aa} shows boundary artifacts which we cut off by len-40. We fit $\log G_{0,\exp(x)-1}$ to a line $A+Bx$ and $\log G_{\exp(x)-1,\exp(x)-1}$ to a line $C+Dx$:

In[**10**]
```
{Fit[Table[{Log[1+xs[[k]]], Log[gs[20][[k]]]}, {k, 1, len}],
       {1, x}, x],
 Fit[Table[{Log[1+xs[[k]]], Log[gfull[20][[k]]]}, {k, 1, len-40}],
       {1, x}, x]}
```

For $\lambda>0$ the general theory leads to undetermined parameters C_{λ,Λ^2} and $f_{\lambda,\Lambda^2}(b)$ in the formula (18) for the 2-point function. In a first step we assume $f_{\lambda,\Lambda^2}(b)=0$ so that

the fixed point equation (32) is unchanged. Under this assumption, C_{λ,Λ^2} is computable from (33) which we implement as

```
In[11] ClL[lis_, hilb_, xi_, a_] := (1 - xi[[a]]/co)*(Exp[
         Hilbert[Table[Tau[lis, hilb, xi, n, a], {n, 1, len+1}],
                xi, 1, len] -
         Hilbert[Table[Tau[lis, hilb, xi, n, 1], {n, 1, len+1}],
                xi, a, len]]*
            Sqrt[(la Pi xi[[a]]/(1 + xi[[a]]))^2 +
            ((1 + la Pi xi[[a]] hilb[[a]])/((1+xi[[a]]) lis[[a]]))^2] -
          1 )/xi[[a]]
```

Fig. 4 shows typical results.

A.3 The Stieltjes property

For a first impression we implement Widder's operators $L_{n,t}$ defined in (36) for $n \geq 1$ via an interpolation formula

```
In[12] WidderInterpolation[xi_, lis_, n_, t_] := (
          (-x)^(n-1)/If[n>=2, n!(n-2)!, 1]*
             D[Interpolation[ Table[{xi[[k]], xi[[k]]^n lis[[k]]},
                             {k, 1, len+1}], InterpolationOrder->2n][x],
                {x, 2n-1}]) /.x->t
```

The discrete list of G_{aa} is interpolated by a polynomial of degree $2n$. Clearly, this is only reliable for small n. We have given typical results in [16, Fig. 3].

The implementation of the integral formula for $L_{n,t}$ starts with the formula (45) for the derivatives $(\log G_{0b})^{(\ell)}$:

```
In[13] DLogG0[ell_, lis_, hilb_, xi_, b_] := (-1)^ell (ell-1)!  *
           (1/(1 + xi[[b]])^ell + Sign[la]* Hilbert[ Table[
               Sin[ell Tau[lis, hilb, xi, k, b]]*(If[k>1,
                   Sin[Tau[lis, hilb, xi, k, b]]/(Abs[la] Pi xi[[k]]),
                        1/(1 + xi[[b]]))]^ell,
                {k, 1, len+1}], xi, 1, len])
```

We arrange them in a table `dlogg[i]` $= \{(\log G_{0b})^{(\ell)}\}_{\ell b}$ of the following type

```
In[14] dlogg[i] = Table[DLogG0[n, gs[i], hs[i], xs, b],
                          {n, 1, 11}, {b, 1, len+1}];
```

Here `[i]` refers to the value reached in **In[8]**, and the length 11 can vary, of course. We compute the derivatives $(G_{0b})^{(n)}$ via (43):

```
In[15] DG0[n_, lis_, dlogg_, b_] := lis[b]*If[n==0, 1, Sum[
           BellY[n, k, Table[dlogg[[m]][[b]], {m, 1, n-k+1}]], {k, 1, n}]]
```

We arrange them in a table `dg[i]` $= \{(G_{0b})^{(n)}\}_{nb}$ of the type

In[16]
```
dg[i] = Table[DG0[n, gs[i], dlogg[i], b],
                        {n, 1, 11}, {b, 1, len+1}];
```

and implement the functions $F^{\Lambda}_{n,k}(a)$ of (49b) and $C^n_0(a)$ of (51) and (50) as

In[17]
```
FSum[n_, k_, xi_, lng_, a_] := (1/(1-xi[[a]]/xi[lng+1]))* (1+
            Sum[(Binomial[n-k-1,p]/ Binomial[n-1,p])*
                 (-xi[[a]]/(xi[[lng+1]]-xi[a]))^p, {p, 1, n-k-1}]);
```

In[18]
```
DCotTau0[n_, lis_, dg_, xi_, a_] := If[a == len+1,
        InterpolatingPolynomial[ Table[xi[[j]],
           DCotTau0[n, lis, dg, xi, j], {j, len-2, len}], xi[[len+1]]],
        (n!/lis[[a]])* (1 + la Pi xi[[a]] Hilbert[lis, xi, a, len])*
           Sum[((-1)^l l!/n!)  BellY[n, l, Table[(-xi[[a]])^kappa *
               dg[[kappa]][[a]]/lis[[a]], {kappa, 1, n-l+1}]],
             {l, 1, n}] +
        (n!/lis[[a]])*Sum[(1 +
             (la xi[[a]]/k)*Sum[ If[l==0, lis[[len+1]],
                    (-xi[[len+1]])^l dg[[l]][[len+1]]/ l!]*
                      FSum[k, l, xi, len, a], {l, 0, k-1}] +
             la Pi xi[[a]]* Hilbert[ Table[(-xi[[c]])^k *
                     dg[[k]][[c]]/k!, {c, 1, len+1}], xi, a, len])*
          If[n==k, 1, Sum[((-1)^l l!/(n-k)!)*
                     BellY[n-k, l, Table[(-xi[[a]])^kappa *
                       dg[[kappa]][[a]]/lis[[a]], {kappa, 1, n-k-l+1}]],
                    {l, 1, n-k}]],
           {k, 1, n}]]
```

The variable length `lng` in `FSum` is necessary for a subsequent step. To avoid "0^0" we have to separately implement the case $p = 0$ in (49b). Since $C^n_0(\Lambda^2) =$`DCotTau0[n, gs[i], dg[i], xs, len+1]` is undefined, we extrapolate it via the quadratic function through its values at `xs[[len-2]]`, `xs[[len-1]]` and `xs[[len]]`. We arrange these functions in a table `dcottau[i]` $= \{C^n_0(a)\}_{na}$ implemented as

In[19]
```
dcottau[i] = Table[DCotTau0[n, gs[i], dg[i], xs, a],
                    {n, 1, 11}, {a, 1, len+1}];
```

The next step consists in implementing the functions $A^{(n,\ell)}$ defined in (52) and $L^{(n,\ell)}$ defined in (53):

In[20]
```
NegXDADaDb[n_, ell_, lis_, hilb_, dg_, dcottau_, xi_, a_, b_] :=
       If[n+ell==0, Tau[lis, hilb, xi, a, b],
        If[ell==0, Sum[((-1)^k (k-1)!/n!)*
          Sin[k Tau[lis, hilb, xi, a, b]] * BellY[n, k, Table[
             (kappa!*xi[[b]] + dcottau[[kappa]][[a]])*
               If[a==1, 1/(1+xi[[b]]),
                   Sin[Tau[lis, hilb, xi, a, b]]/(Abs[la] Pi xi[[a]])],
```

```
                {kappa, 1, n-k+1}]],
      {k, 1, n}],
    Sum[Binomial[n-m+ell-1, ell-1] ((-1)^k (ell+k-1)!/(m!  ell!))*
      Sin[(ell+k) Tau[lis, hilb, xi, a, b]] *
      (xi[[b]]* If[a==1, 1/(1+xi[[b]]),
        Sin[Tau[lis, hilb, xi, a, b]]/(Abs[la] Pi xi[[a]])])^ell*
      BellY[m, k, Table[(kappa!*xi[[b]] + dcottau[[kappa]][[a]])*
          If[a==1, 1/(1+xi[[b]]),
            Sin[Tau[lis, hilb, xi, a, b]]/(Abs[la] Pi xi[[a]])],
          {kappa, 1, m-k+1}]],
     {m, 0, n}, {k, 0, m}] ]]
```

In[21]
```
NegXDLDaDb[n_, ell_, lis_, hilb_, dg_, dcottau_, xi_, a_, b_] :=
   If[n+ell==0, Log[If[a==1, 1/(1+xi[[b]]),
      Sin[Tau[lis, hilb, xi, a, b]]/(Abs[la] Pi xi[[a]])]],
    If[ell==0, 1/n + Sum[((-1)^k (k-1)!/n!)*
      Cos[k Tau[lis, hilb, xi, a, b]] * BellY[n, k, Table[
        (kappa!  xi[[b]] + dcottau[[kappa]][[a]])*
          If[a==1, 1/(1+xi[[b]]),
              Sin[Tau[lis, hilb, xi, a, b]]/(Abs[la] Pi xi[[a]])],
            {kappa, 1, n-k+1}]],
      {k, 1, n}],
    Sum[Binomial[n-m+ell-1, ell-1] ((-1)^k (ell+k-1)!/(m!  ell!))*
      Cos[(ell+k) Tau[lis, hilb, xi, a, b]] *
      (xi[[b]]* If[a==1, 1/(1+xi[[b]]),
        Sin[Tau[lis, hilb, xi, a, b]]/(Abs[la] Pi xi[[a]])])^ell*
      BellY[m, k, Table[(kappa!*xi[[b]] + dcottau[[kappa]][[a]])*
          If[a==1, 1/(1+xi[[b]]),
            Sin[Tau[lis, hilb, xi, a, b]]/(Abs[la] Pi xi[[a]])],
          {kappa, 1, m-k+1}]],
     {m, 0, n}, {k, 0, m}] ]]
```

According to (54), the derivatives $\frac{(-a)^n(-b)^\ell}{n!\ell!}\frac{\partial^{n+\ell}(\log G_{ab})}{\partial a^n \partial b^\ell}$ are a sum of $L^{(n,\ell)}(a,b)$ defined before and the more complicated remainder $\frac{(-a)^n(-b)^\ell}{n!\ell!}\frac{\partial^{n+\ell}(\mathrm{sign}(\lambda)\mathcal{H}_a^{\tilde\Lambda}[\tau_b(\bullet)])}{\partial a^n \partial b^\ell}$. The latter function is for $n+\ell>0$ and $a<\tilde\Lambda^2=$ `lng` implemented as

In[22]
```
NegXDHTauDaDb[n_,ell_,lis_,hilb_,dg_,dcottau_,xi_,lng_,a_,b_] :=
   If[n==0, Sign[la] Hilbert[ Table[
        NegXDADaDb[0, ell, lis, hilb, dg, dcottau, xi, bu, b],
       {bu, 1, lng+1}], xi, a, lng],
    la Pi xi[[a]] Hilbert[ Table[If[bu==1, If[n<=1,
      (-1)^n If[ell==0, 1, xi[[b]]^ell]/(1 + xi[[b]])^(ell+1), 0],
      NegXDADaDb[n,ell,lis,hilb,dg,dcottau,xi,bu,b]/
                  (Abs[la] Pi xi[[bu]])],
```

```
 {bu, 1, lng+1}], xi, a, lng] -
(Sign[la]/(Pi n))*(-xi[[a]]/(xi[[lng+1]] - xi[[a]]))^n *
       NegXDADaDb[0, ell, lis, hilb, dg, dcottau, xi, a, b] +
If[n<=1, 0, (Sign[la]/(Pi *n(n-1)))*(xs[[a]]/xs[[lng+1]]) *
     Sum[k*NegXDADaDb[k,ell,lis,hilb,dg,dcottau,xi,lng+1,b]*
       FSum[n-1, k-1, xi, lng, a] , {k, 1, n-1}]]]
```

The 6th line `(-1)^n If[...]` uses the limit (B.3).

We intercept the cases $n + \ell = 0$ and $a < \tilde{\Lambda}^2$ to obtain the following implementation of $\frac{(-a)^n(-b)^\ell}{n!\ell!}\frac{\partial^{n+\ell}(\log G_{ab})}{\partial a^n \partial b^\ell}$:

In[23]
```
NegXDLogGDaDb[n_,ell_,lis_,hilb_,dg_,dcottau_,xi_,lng_,a_,b_] :=
 If[a==lng+1, InterpolatingPolynomial[ Table[{xi[[j]],
      NegXDLogGDaDb[n,ell,lis,hilb,dg,dcottau,xi,lng,j,b]},
   {j, lng-2, lng}], xi[[lng+1]]],
 If[n+ell==0, Log[Gfull[lis, hilb, xi, a, b]],
 NegXDHTauDaDb[n, ell, lis, hilb, dg, dcottau, xi, lng, a, b] +
 NegXDLDaDb[n, ell, lis, hilb, dg, dcottau, xi, a, b] ]]
```

It remains to sum these contributions to $(-a)^n(\log G_{aa})^{(n)}$ according to (55c):

In[24]
```
NegXDLogGfull[n_, lis_, hilb_, dg_, dcottau_, xi_, lng_, a_] :=
 n!*Sum[NegXDLogGDaDb[n-ell,ell,lis,hilb,dg,dcottau,xi,lng,a,a],
    {ell, 0, n}]
```

We collect these values in a table and use Faà di Bruno to obtain $(-a)^n(G_{aa})^{(n)}$ according to (55b):

In[25]
```
negxdloggfull[i]=Table[
   NegXDLogGfull[n, gs[i], hs[i], dg[i], dcottau[i],xs,1200,a],
      {n, 1, 11}, {a, 1, 200}];
 negxdgfull[i] = Table[
   DGO[n, gfull[i], negxdloggfull[i], a], {n, 1, 11}, {a, 1, 200}];
```

The sizes `n=1...11` and `a=1...200` can be adapted, of course, but require the tables `dg[i]` defined in **In[16]** and `dcottau[i]` defined in **In[19]** of length not shorter than `n`. Also the secondary cutoff $\tilde{\Lambda}^2 = x_{1201}$ can be adapted. It remains to define the integral formula for Widder's operators $L_{n,t}[G_{\bullet\bullet}]$ according to (55a) and to visualise the results:

In[26]
```
WidderL[n_, t_, tab_] := Sum[((-1)^(n-l) *
   Binomial[2n-1, l] Binomial[n, l] l!/ If[n<=1, 1, (n-2)!  n!])*
      tab[[2n-l-1]][[t]], {l, 0, n}]
```

In[27]
```
ListPlot[{
   Table[{xs[[k]], WidderL[2, k, negxdgfull[i]]}, {k, 1, 200}],
   Table[{xs[[k]], WidderL[3, k, negxdgfull[i]]}, {k, 1, 200}],
   Table[{xs[[k]], WidderL[4, k, negxdgfull[i]]}, {k, 1, 200}],
   Table[{xs[[k]], WidderL[5, k, negxdgfull[i]]}, {k, 1, 200}],
```

```
Table[{xs[[k]], WidderL[6, k, negxdgfull[i]]}, {k, 1, 200}]}]
```

Typical results are shown in figs. 11 and 14. Figs. 12 and 13 compare `WidderL` with `WidderInterpolation` defined in **In**[**12**]. Note that `WidderL[s,...]` requires lengths `n=2s-1` or bigger in **In**[**14**], **In**[**16**], **In**[**19**] and **In**[**25**]. For comparison (table 6 and fig. 10) we can evaluate $L_{n,t}[G_{0\bullet}]$ starting from `dlogg[i]` computed in **In**[**14**] as follows:

In[**28**]
```
negxdg0[i] = Table[DG0[n, gs[i], Table[
               (-xs[[a]])^k dlogg[i][[k]][[a]],{k, 1, Length[dlogg[i]]}],
         {n, 1, 11}, {a, 1, 200}];
     Table[{xs[[k]], WidderL[6, k, negxdg0[i]]}, {k, 1, 200}]
```

B The derivatives $L^{(n,\ell)}(a,b)$ and $(A^{(n,\ell)}(a,b))/(|\lambda|\pi a)$ at $a=0$

Vanishing of Widder's operators $L_{n,t}[G_{\bullet\bullet}]$ at $t=0$ requires $L^{(n,\ell)}(0,b)=0$ for the functions (53). With $\tau_b(0)=0$, $\lim_{a\to0}\frac{\sin(\tau_b(a))}{|\lambda|\pi a}=\frac{1}{1+b}$ and $\lim_{a\to0}\frac{C_b^k(a)\sin(\tau_b(a))}{|\lambda|\pi a}=k!$ as well as $Y_{m,k}(1!,2!,\dots,(m-k+1)!)=\frac{m!(m-1)!}{k!(k-1)!(m-k)!}$ for $m\ge1$ [18], we have:

$$
\begin{aligned}
&L^{(n,\ell)}(0,b)\big|_{\ell,n\ge1}\\
&=\Big(\frac{b}{1+b}\Big)^{\ell}\sum_{m=0}^{n}\sum_{k=0}^{m}\binom{n-m+\ell-1}{\ell-1}\frac{(-1)^k(\ell+k-1)!}{m!\ell!}Y_{m,k}\Big(1!,2!,\dots,(m-k+1)!\Big)\\
&=\Big(\frac{b}{1+b}\Big)^{\ell}\Big\{\frac{(n+\ell-1)!}{n!\ell!}-\sum_{m=1}^{n}\binom{n-m+\ell-1}{\ell-1}\sum_{k=0}^{m-1}\frac{(-1)^k1!(\ell+k)!(m-1)!}{(k+1)!\ell!(m-1-k)!k!}\Big\}\\
&=\Big(\frac{b}{1+b}\Big)^{\ell}\Big\{\frac{(n+\ell-1)!}{n!\ell!}-\sum_{m=1}^{n}\binom{n-m+\ell-1}{\ell-1}\,{}_2F_1\Big(\begin{matrix}\ell+1,1-m\\2\end{matrix}\Big|1\Big)\Big\}\,.
\end{aligned}
\tag{B.1}
$$

Now we use the recursion formula [17, §9.137.7] to obtain

$${}_2F_1\Big(\begin{matrix}\ell+1,1-m\\2\end{matrix}\Big|1\Big)=\Big(\prod_{p=2}^{m}\Big(1-\frac{\ell+1}{p}\Big)\Big){}_2F_1\Big(\begin{matrix}\ell+1,m-m\\1+m\end{matrix}\Big|1\Big)=\frac{(-1)^{m-1}(\ell-1)!}{(\ell-m)!m!}\,.$$

The remaining m-summation in (B.1), including the $m=0$ case $\frac{(n+\ell-1)!}{n!\ell!}$, yields

$$L^{(n,\ell)}(0,b)\big|_{\ell,n\ge1}=\Big(\frac{b}{1+b}\Big)^{\ell}\frac{(n+\ell-1)!}{n!\ell!}\,{}_2F_1\Big(\begin{matrix}-n,-\ell\\1-n-\ell\end{matrix}\Big|1\Big)=0\,,$$

using [17, §9.137.7] again. The proof of $L^{(n,0)}(0,b)=0$ is much simpler.

For the numerical implementation we have to control the function under the Hilbert transform in (54) at $\bullet=0$. The same considerations as before yield

$$\lim_{a\to0}\frac{A^{(n,\ell)}(a,b)}{|\lambda|\pi a}\Big|_{\ell,n\ge1}$$

$$
\begin{aligned}
&= \Big(\frac{b}{1+b}\Big)^{\ell} \sum_{m=0}^{n} \sum_{k=0}^{m} \binom{n-m+\ell-1}{\ell-1} \frac{(-1)^k(\ell+k)!}{m!\ell!} Y_{m,k}\Big(1!, 2!, \dots, (m-k+1)!\Big) \\
&= \Big(\frac{b}{1+b}\Big)^{\ell} \Big(\binom{n+\ell-1}{\ell-1} - (\ell+1) \sum_{m=1}^{n} \binom{n-m+\ell-1}{\ell-1} \sum_{k=0}^{m-1} \frac{(-1)^k(\ell+1+k)!1!(m-1)!}{(\ell+1)!(k+1)!(m-1-k)!k!} \Big) \\
&= \Big(\frac{b}{1+b}\Big)^{\ell} \Big(\binom{n+\ell-1}{\ell-1} - (\ell+1) \sum_{m=1}^{n} \binom{n-m+\ell-1}{\ell-1} {}_2F_1\Big(\begin{matrix}\ell+2, 1-m \\ 2\end{matrix}\Big|1\Big) \Big) \\
&= \Big(\frac{b}{1+b}\Big)^{\ell} \sum_{m=0}^{n} \binom{n-m+\ell-1}{\ell-1} \frac{(-1)^m(\ell+1)!}{(\ell+1-m)!m!} \\
&= \Big(\frac{b}{1+b}\Big)^{\ell} \frac{(n+\ell-1)!}{n!(\ell-1)!} \sum_{m=0}^{n} \frac{(-1)^m(\ell+1)!(n+\ell-1-m)!n!}{(\ell+1-m)!(n+\ell-1)!(n-m)!m!} \\
&= \begin{cases} \Big(\frac{b}{1+b}\Big) \sum_{m=0}^{n} \frac{(-1)^m 2!}{(2-m)!m!} & \text{for } \ell = 1 \ , \\ \Big(\frac{b}{1+b}\Big)^{\ell} \frac{(n+\ell-1)!}{n!(\ell-1)!} {}_2F_1\Big(\begin{matrix}-(\ell+1), -n \\ 1-(n+\ell)\end{matrix}\Big|1\Big) & \text{for } \ell > 1 \ . \end{cases}
\end{aligned}
\tag{B.2}
$$

For $n = 2$ we have ${}_2F_1\big(\begin{smallmatrix}-(\ell+1),-2 \\ -(\ell+1)\end{smallmatrix}\big|1\big) = 0$ and thus from the recursion [17, §9.137.7] ${}_2F_1\big(\begin{smallmatrix}-(\ell+1),-n \\ 1-(n+\ell)\end{smallmatrix}\big|1\big) = 0$ for all $n \geq 2$. The cases $n = 1$ and $n = 0$ can easily be discussed so that in summary we obtain

$$
\lim_{a\to 0} \frac{A^{(n,\ell)}(a,b)}{|\lambda|\pi a} = \Big(\frac{b}{1+b}\Big)^{\ell} \cdot \begin{cases} (-1)^n & \text{for } n \in \{0,1\} \ , \\ 0 & \text{for } n \geq 2 \ . \end{cases}
\tag{B.3}
$$

Repeating these arguments for (52b) we find that (B.3) also holds for $\ell = 0$.

References

[1] H. Grosse and R. Wulkenhaar, "Renormalisation of ϕ^4-theory on noncommutative $\mathbb{R}^4$ in the matrix base," Commun. Math. Phys. **256** (2005) 305–374 [hep-th/0401128].

[2] H. Grosse and R. Wulkenhaar, "The β-function in duality-covariant noncommutative ϕ^4-theory," Eur. Phys. J. C **35** (2004) 277–282 [hep-th/0402093].

[3] M. Disertori and V. Rivasseau, "Two and three loops beta function of non commutative ϕ_4^4 theory," Eur. Phys. J. C **50** (2007) 661–671 [hep-th/0610224].

[4] M. Disertori, R. Gurau, J. Magnen and V. Rivasseau, "Vanishing of beta function of non commutative ϕ_4^4 theory to all orders," Phys. Lett. B **649** (2007) 95–102 [hep-th/0612251].

[5] H. Grosse and R. Wulkenhaar, "Progress in solving a noncommutative quantum field theory in four dimensions," arXiv:0909.1389 [hep-th].

[6] H. Grosse and R. Wulkenhaar, "Self-dual noncommutative ϕ^4-theory in four dimensions is a non-perturbatively solvable and non-trivial quantum field theory," Commun. Math. Phys. **329** (2014) 1069–1130 [arXiv:1205.0465 [math-ph]].

[7] T. Carleman, "Sur la résolution de certaines équations intégrales," Arkiv for Mat., Astron. och Fysik **16** (1922), 19pp.

[8] F. G. Tricomi, *Integral equations*, Interscience, New York (1957).

[9] N. I. Muskhelishvili, *Singuläre Integralgleichungen*, Akademie-Verlag Berlin (1965).

[10] H. Grosse and R. Wulkenhaar, "Solvable limits of a 4D noncommutative QFT," arXiv:1306.2816 [math-ph].

[11] K. Osterwalder and R. Schrader, "Axioms for Euclidean Green's functions," Commun. Math. Phys. **31** (1973) 83–112.

[12] K. Osterwalder and R. Schrader, "Axioms for Euclidean Green's functions II," Commun. Math. Phys. **42** (1975) 281–305.

[13] D. V. Widder, "The Stieltjes transform," Trans. Amer. Math. Soc. **43** (1938) 7–60.

[14] H. Grosse and R. Wulkenhaar, "On the fixed point equation of a solvable 4D QFT model," arXiv:1505.05161 [math-ph].

[15] C. Berg, "Stieltjes-Pick-Bernstein-Schoenberg and their connection to complete monotonicity," in: *Positive definite functions. From Schoenberg to space-time challenges*, eds J. Mateu and E. Porcu, Dept. of Mathematics, University Jaume I, Castellon, Spain (2008).

[16] H. Grosse and R. Wulkenhaar, "Construction of the Φ^4_4-quantum field theory on noncommutative Moyal space," RIMS Kôkyûroku 1904 (2014) 67–104 [arXiv:1402.1041 [math-ph]].

[17] I.S. Gradshteyn and I. M. Ryzhik, *Table of integrals, series, and products*, Academic Press (1994).

[18] Encyclopaedia of mathematics, `http://www.encyclopediaofmath.org/index.php/Bell_polynomial`

[19] R. F. Streater and A. S. Wightman, *PCT, spin and statistics, and all that,* Benjamin, New York (1964).

[20] J. Moser, "Three integrable Hamiltonian systems connnected with isospectral deformations," Adv. Math. **16** (1975) 197.

[21] P. P. Kulish, "Factorization of the classical and quantum S matrix and conservation laws," Theor. Math. Phys. **26** (1976) 132 [Teor. Mat. Fiz. **26** (1976) 198].

[22] S. Okada and D. Elliott, "Hölder continuous functions and the finite Hilbert transform," Math. Nachr. **169** (1994) 219–233.